

**$\mathbf{k} \cdot \mathbf{p}$  model for the energy dispersions and absorption spectra of InAs/GaSb type-II superlattices**

Y. Livneh\*

*Department of Electrical Engineering–Physical Electronics, Faculty of Engineering, Tel Aviv University, Ramat-Aviv, 69978, Israel*P. C. Klipstein,<sup>†</sup> O. Klin, N. Snapi, S. Grossman, A. Glozman, and E. Weiss*Semiconductor Devices, P. O. Box 2250, Haifa 31021, Israel*

(Received 1 May 2012; revised manuscript received 7 August 2012; published 20 December 2012)

We have fitted the  $\mathbf{k} \cdot \mathbf{p}$  model derived recently by one of the authors [Klipstein, *Phys. Rev. B* **81**, 235314 (2010)] to experimentally measured photoabsorption spectra at 77 and 300 K for representative InAs/GaSb superlattices with band-gap wavelengths between 4.3 and 10.5  $\mu\text{m}$ . The model is able to reproduce the main features of the absorption spectra, including a strong peak from the zone boundary  $\text{HH}_2 \rightarrow E_1$  transition. We have also used the same model to predict the band-gap wavelengths of over 30 more superlattices, measured by photoluminescence spectroscopy. The maximum error is 0.6  $\mu\text{m}$ , which corresponds to an uncertainty of less than 0.4 ML in layer width. This is comparable with the experimental uncertainty in layer widths, determined by *in situ* beam-flux measurements in the growth reactor. By eliminating all terms from the Hamiltonian, the energy contribution of which is less than the error due to the uncertainty in layer widths, the number of unknown fitting parameters has been reduced to six: two Luttinger parameters, three interface parameters, and the valence band offset. The remaining four Luttinger parameters are not independent and are determined from the two independent ones. Our set of Luttinger parameters is close to that reported by Lawaetz [*Phys. Rev. B* **4**, 3460 (1971)], with a maximum deviation in any parameter of 0.6. The interface parameters are diagonal and have values of  $D_S = 3 \text{ eV \AA}$ ,  $D_X = 1.3 \text{ eV \AA}$ , and  $D_Z = 1.1 \text{ eV \AA}$  at 77 K. The off-diagonal interface parameters  $\alpha$  and  $\beta$  are too small to be fitted with any accuracy and have negligible effect on the unpolarized photoabsorption spectra. We also propose values for the room-temperature Luttinger and interface parameters. The fitted unstrained InAs/GaSb band overlap is 0.142 eV.

DOI: [10.1103/PhysRevB.86.235311](https://doi.org/10.1103/PhysRevB.86.235311)

PACS number(s): 73.21.Cd, 71.15.-m, 73.61.Ey

**I. INTRODUCTION**

The  $\mathbf{k} \cdot \mathbf{p}$  model is perhaps one of the simplest and most accessible methods for calculating the electronic structure and physical properties of a wide range of inorganic semiconductors. Sometimes referred to as the “standard model,”<sup>1</sup> it has gained wide popularity because it can be considered to be a generalization of the familiar one-band effective mass approach. In a recent *ad hoc* survey, Cardona estimated that about 1500 articles bearing the term  $\mathbf{k} \cdot \mathbf{p}$  in the title can be found in literature bases, and that they have been cited about 15 000 times.<sup>2</sup>

While the application of the  $\mathbf{k} \cdot \mathbf{p}$  model to bulk semiconductor materials is fairly straightforward, for example, in the form of the Kane<sup>3</sup> or Luttinger-Kohn<sup>4</sup> Hamiltonians, its formal application to semiconductor microstructures such as superlattices and quantum wires has been the subject of wider discussion. This is due, in part, to some uncertainty over the precise boundary conditions to use for the envelope functions at an interface between different semiconductor materials. For nearly lattice matched materials, an important step towards the resolution of this problem was to derive the envelope-function equations using zone-center Bloch functions  $u_n(\mathbf{r})$  from a bulk reference crystal as the basis states, and to treat the difference between the microscopic potentials of the real heterostructure and the reference crystal as a spatially dependent perturbation  $\delta V(\mathbf{r})$ .<sup>5</sup> In the early 1990s, Burt used this approach to express the Schrödinger equation in terms of its Fourier components, and produced a set of coupled envelope-function equations which included terms of the form  $\Omega_{nn'}\delta(z - z_i)$  for interfaces located at  $z_i$ .<sup>6</sup> The mixing potential  $\Omega_{nn'}$  was shown to depend on the microscopic potential at the interface and the Bloch

functions  $u_n(\mathbf{r})$  and  $u_{n'}(\mathbf{r})$  of the reference crystal. It took the simple form  $\Omega_{nn'} = \langle n | \delta V | n' \rangle$  and described zone-center mixing between states of different symmetry.<sup>7</sup> Subsequently, Foreman<sup>8</sup> calculated typical values for the mixing potential in a number of cases, including the mixing between heavy- and light-hole valence states, or between conduction band electrons and valence band light holes. It should be noted that the mixing between heavy and light holes was first predicted explicitly in 1992 by Aleiner and Ivchenko, based on an analysis of the interface symmetry.<sup>9</sup>

Burt proposed that in the bulk regions of a superlattice, a piecewise Kane- or Luttinger-type Hamiltonian could be used, provided that the quadratic valence band terms were properly “symmetrized.” Foreman<sup>10</sup> implemented Burt’s prescription in a six-band Kane model to show that terms of the form  $Nk_z k_x$  should be replaced with  $k_z D k_x + k_x H_1 k_z$ , or its Hermitian conjugate, where  $D = F - G$  and  $F$ ,  $H_1$ , and  $G$  are the Kane parameters associated with the remote  $s$ ,  $p$ , and  $d$  bands, respectively.<sup>3</sup> Foreman also derived a six-band Luttinger-type Hamiltonian by adding the spin-orbit interaction and transforming to a basis of heavy, light and spin-orbit split-off hole states. A consequence of the Burt-Foreman symmetrized term  $k_z D k_x + k_x H_1 k_z$  is that it leads to an additional interface contribution proportional to  $k_x \Delta D$ .

The Burt-Foreman treatment did not deal with symmetrization of the  $Pk_z$  terms, associated with the  $\mathbf{k} \cdot \mathbf{p}$  interaction between conduction and valence states in the eight-band case. Also, as pointed out by Takhtamirov and Volkov in 1997,<sup>11</sup> their treatment was not consistent in which of the second-order perturbation terms it included, and which it omitted. These terms are of magnitude  $\delta \vec{V}(\vec{k}a)^\ell$  with  $\ell = 2$ , where  $\delta \vec{V}$  is a

typical band offset,  $\hbar\bar{k}$  is the average momentum modulus of the envelope function, and  $a$  is the bulk lattice parameter.<sup>12</sup> Nevertheless, the Burt-Foreman treatment has become widely adopted, presumably because of its simplicity and because effects related to the interface band mixing potentials have been observed experimentally.<sup>13–16</sup> In fact, it can be argued that the Burt-Foreman model with only the addition of a properly symmetrized  $Pk_z$  term provides a satisfactory approach for fitting experimental data in common atom superlattices, such as GaAs/AlGaAs, to an eight-band model. Since a fluctuation of just one monolayer at constant superlattice period already introduces an error of order  $\ell = 1$ ,<sup>17</sup> the inclusion of higher-order terms in the model is of questionable value.

In 1975, Leibler<sup>18</sup> used the Luttinger-Kohn<sup>4</sup> basis to consider the effect of a slow composition variation, such as might occur when the relative proportion of two materials, A and B, in a semiconductor alloy is varied with position. His approach was extended by Takhtamirov and Volkov<sup>19,20</sup> to the case of a semiconductor superlattice where the composition is switched abruptly and periodically between materials A and B. Following Leibler's approach, they defined a composition modulation function  $G(z)$  to describe the composition variation in the growth direction such that  $\delta V(\mathbf{r}) = G(z)[U_B(\mathbf{r}) - U_A(\mathbf{r})] = G(z)\delta U$ , and  $U_A(\mathbf{r})$ ,  $U_B(\mathbf{r})$  are the microscopic potentials of materials A and B, respectively. They derived a general envelope-function equation in reciprocal space, but only considered the real-space envelope-function equation in detail for a single conduction band.

Although the treatment turns out to be somewhat cumbersome, one of the authors recently used the Takhtamirov and Volkov approach to derive real-space Kane-type Hamiltonians for both six and eight bands.<sup>17</sup> In that derivation, all of the important terms up to  $\ell = 2$  were included. Expressions were derived for the symmetrization of the  $Nk_z k_x$  and  $Pk_z$  terms, which are not the same as Burt's. A number of additional interface terms were also introduced. It was shown that in an ideal no common atom superlattice,  $G'(z)$  contains an antisymmetric part that is essentially absent in an ideal common atom superlattice, and that this leads to large, diagonal, first-order interface terms. Moreover, the off-diagonal terms are expected to be smaller than those typical of a common atom superlattice. Another useful feature that emerged in the derivation was a demonstration that only two out of the six Luttinger parameters needed to define the superlattice Hamiltonian are independent, and that they can be used to calculate the other four, without compromising on accuracy up to order  $\ell = 2$ . As will be demonstrated in this work, this provides a considerable reduction in the number of adjustable fitting parameters that are needed to make a comparison with experimental data, and it should thus lead to a more reliable result. In the following, we shall refer to the eight-band form of the Hamiltonian as the Takhtamirov-Volkov-Klipstein-8 Hamiltonian, or TVK8.

The aim of this work is to compare the TVK8 Hamiltonian with experimental data, for no common atom type-II superlattices (T2SLs) in which A = InAs and B = GaSb. Such InAs/GaSb superlattices were first proposed by Sai-Halacz, Tsu, and Esaki<sup>21</sup> in 1977 and are of current interest for a

number of applications, including as a possible alternative to mercury cadmium telluride for infrared detection.<sup>22–24</sup> We consider a wide range of superlattice band-gap energies, and also examine the well-known blue-shift of the band gap with increasing GaSb thickness when the InAs thickness is kept constant.<sup>25</sup> It was previously claimed that the  $\mathbf{k} \cdot \mathbf{p}$  method can not reproduce this effect.<sup>26</sup> We show here that the TVK8 formulation of the theory succeeds very well at reproducing not only the blue-shift of the band gap, but also the whole absorption spectrum over a useful energy range, including a strong feature due to zone boundary transitions between the second heavy-hole band and the first electron band.

Our approach is as follows. We begin by calculating the photoabsorption spectra for several representative superlattices, at 77 or 300 K, in order to find a single set of six independent Luttinger and interface parameters that can produce a reasonable fit to the data at each temperature. Using the same 77-K parameters, we then compare the band gaps determined by low-temperature photoluminescence measurements with those predicted by the model, for about 30 more superlattices in which the InAs and GaSb layer widths have been determined independently. All other parameters used in the model, apart from the layer widths, can be determined independently, and with sufficient accuracy, from x-ray, spectroscopic, and mechanical measurements, and are taken from well-established literature databases.<sup>27,28</sup> The method of layer-width determination is based on *in situ* beam-flux measurements in the molecular beam epitaxy reactor used to grow the structures, combined with x-ray diffraction measurements of the superlattice period. We show that the TVK8 model agrees with all of the experimental absorption and photoluminescence data, to within an uncertainty of  $\pm 0.4$  ML in any layer width, for band-gap photon wavelengths spanning 4.3 to 12  $\mu\text{m}$ . The fitted Luttinger parameters are close to those originally proposed by Lawaetz,<sup>29</sup> while the large diagonal and small off-diagonal parameters deduced for the first-order interface matrix are consistent with the expected behavior of the TVK8 Hamiltonian.

The arrangement of this paper is now described. In Sec. II, the TVK8 Hamiltonian is introduced and terms below the desired degree of accuracy are eliminated. In Sec. III, we introduce a method for solving the Hamiltonian and calculating the absorption coefficient of the superlattice. The experimental methods of photoluminescence spectroscopy, spectral absorption, and layer-width determination are presented in Sec. IV. These layer widths are used in Sec. V to calculate energy dispersions and absorption spectra. The quality of the agreement between the calculated band gaps and absorption spectra and their experimental determinations is discussed in Sec. VI. We present our conclusions in Sec. VII.

## II. THE HAMILTONIAN

Our calculation is based on the standard spin-orbit Hamiltonian  $H_{\text{SO}}$ , as quoted for example in Eq. (5) of Ref. 30, to which is added the following  $8 \times 8$  Hamiltonian matrix made up of two diagonal blocks  $\mathbf{M}$ , one for each spin direction,

where  $\mathbf{M} = \mathbf{M}_1 + \mathbf{M}_{\text{IF}} + \mathbf{M}_{\text{strain}}$ :

$$\mathbf{M}_1 = \begin{bmatrix} \{A'(k_x^2 + k_y^2) + k_z A' k_z + E_C\} & iPk_x & iPk_y & i\{(1-f)Pk_z + fk_z P\} \\ -iPk_x & \{Lk_x^2 + Mk_y^2 + k_z Mk_z + E_v\} & Nk_x k_y & Nk_x k_z \\ -iPk_y & Nk_x k_y & \{Mk_x^2 + Lk_y^2 + k_z Mk_z + E_v\} & Nk_y k_z \\ -i\{fPk_z + (1-f)k_z P\} & Nk_x k_z & Nk_y k_z & \{M(k_x^2 + k_y^2) + k_z Lk_z + E_v\} \end{bmatrix}, \quad (1)$$

$$\mathbf{M}_{\text{IF}} = \sum_i \delta(z - z_i) \begin{bmatrix} D_S & 0 & 0 & \pi_i \beta \\ 0 & D_X & \pi_i \alpha & 0 \\ 0 & \pi_i \alpha & D_X & 0 \\ \pi_i \beta & 0 & 0 & D_Z \end{bmatrix}, \quad (2)$$

$$\mathbf{M}_{\text{strain}} = \begin{bmatrix} a_c(2\epsilon_{\parallel} + \epsilon_{\perp}) & -iP\epsilon_{\parallel} k_x & -iP\epsilon_{\parallel} k_y & -iP\epsilon_{\perp} k_z \\ iP\epsilon_{\parallel} k_x & \{a_v(2\epsilon_{\parallel} + \epsilon_{\perp}) + b(\epsilon_{\parallel} - \epsilon_{\perp})\} & 0 & 0 \\ iP\epsilon_{\parallel} k_y & 0 & \{a_v(2\epsilon_{\parallel} + \epsilon_{\perp}) + b(\epsilon_{\parallel} - \epsilon_{\perp})\} & 0 \\ iP\epsilon_{\perp} k_z & 0 & 0 & \{a_v(2\epsilon_{\parallel} + \epsilon_{\perp}) - 2b(\epsilon_{\parallel} - \epsilon_{\perp})\} \end{bmatrix}. \quad (3)$$

A full description of the matrices  $\mathbf{M}_1$  and  $\mathbf{M}_{\text{IF}}$  is given in Ref. 17, while  $\mathbf{M}_{\text{strain}}$  is based on Ref. 31.  $A'$ ,  $L$ ,  $M$ ,  $N$ , and  $P$  are the standard Kane  $\mathbf{k} \cdot \mathbf{p}$  parameters,<sup>3</sup> and  $a_c$ ,  $a_v$ , and  $b$  are the standard Pikus-Bir deformation potentials.<sup>31</sup>  $\epsilon_{\parallel}$  and  $\epsilon_{\perp}$  are strains parallel and perpendicular to the superlattice layers.  $\alpha$ ,  $\beta$ , and the  $D$  parameters are interface-related parameters, the first two of which change sign at normal and inverted interfaces according to the parameter  $\pi_i$  which takes values of  $\pm 1$ .  $f$  is a ‘‘symmetrization’’ parameter which also introduces an interface contribution proportional to the change in the bulk parameter  $P$  at each interface. Note that  $P = \hbar \sqrt{\frac{E_p}{2m_0}}$ , where  $m_0$  is the free electron mass.

The Hamiltonian matrix  $\mathbf{M}$  is the TVK8 Hamiltonian in which all of the  $\ell = 2$  perturbation terms have been omitted. The reason for this is that their contribution is easily masked by layer-width fluctuations of just a few tenths of a monolayer. It will be demonstrated in Sec. IV that we are able to define the layer widths experimentally to a typical accuracy of about  $\pm 0.2$  ML, which is the standard deviation in a statistical distribution of about 30 samples. In Sec. VI, we also perform a direct estimation of the contribution to the band-gap energy of the leading second-order interface terms that have been omitted, where it is shown that their contribution is equivalent to a thickness change of less than 0.3 ML. As expected, this is comparable with our experimental level of accuracy, thereby confirming that the omission of these terms is justified.

Terms of the form  $Nk_x k_z$  in Eq. (1) have not been expressed in their ‘‘symmetrized’’ form because the interface contribution due to the symmetrization is very small in an  $8 \times 8$  model and below our stated level of accuracy. In principle, the  $f$ -symmetrization parameter can make a contribution of order

$\ell = 1$ , and so it has been included formally in Eq. (1). However, it should be noted that for the InAs/GaSb superlattices considered in this work,  $\Delta P \approx 0$  (see Appendix B). The interface contribution due to  $\Delta P$  is therefore quite negligible in our case, and we simply choose a convenient value of  $f = 0.5$ . Finally, we have not included any relativistic terms in the Hamiltonian matrix since even the  $\ell = 1$  relativistic terms are estimated to be significantly smaller than the equivalent nonrelativistic ones.<sup>17</sup>

The spin-orbit matrix and the matrices  $\mathbf{M}_1$  and  $\mathbf{M}_{\text{strain}}$  are piecewise matrices whose parameter values change from layer to layer, while the interface matrix  $\mathbf{M}_{\text{IF}}$  has parameters whose values depend on both superlattice materials, and some of whose signs  $\pi_i$  depend on the way in which they are ordered. As mentioned in the Introduction, the diagonal elements in the interface matrix  $\mathbf{M}_{\text{IF}}$  are expected to be quite large for an ideal InAs/GaSb superlattice, while the off-diagonal elements are expected to be significantly smaller. For example,  $D_S$  has the form  $\langle S | \Phi_0^a \cdot \delta U | S \rangle$ , in which  $|S\rangle$  is the antibonding  $s$ -orbital crystal periodic function of the reference crystal, with analogous expressions for  $D_X$  and  $D_Z$ . The off-diagonal elements have the form  $\alpha = \langle X | \Phi_0^s \cdot \delta U | Y \rangle$  and  $\beta = \langle S | \Phi_0^s \cdot \delta U | Z \rangle$ . The interface matrix thus depends on the two functions  $\Phi_0^a$  and  $\Phi_0^s$ , which were derived and plotted at the end of Ref. 17.  $\Phi_0^a$  is an even function whose amplitude is about five times greater than that of  $\Phi_0^s$ , which is an odd function. This suggests that typical values for  $D_S$ ,  $D_X$ , and  $D_Z$  should be significantly larger than those for  $\alpha$  and  $\beta$ .

It is well known that the interfaces can be grown with either ‘‘InSb’’-like or ‘‘GaAs’’-like bonding, depending on the shutter or valve sequence used in the growth reactor. These two

interface types are represented by two sets of values for the elements in the interface matrix  $\mathbf{M}_{\text{IF}}$ . In this work, we consider only InSb-like interfaces. It should be noted that some authors have tried to treat the interface without an interface matrix, simply by inserting the appropriate bulk Hamiltonian matrix for a single extra monolayer of InSb or GaAs, in a piecewise treatment.<sup>32</sup> This approach can not be correct for a number of reasons. First, a two-dimensional (2D) monolayer does not have the same band-edge energies as a three-dimensional (3D) bulk layer. Second, the derivation of the real-space  $\mathbf{k} \cdot \mathbf{p}$  equation [Eq. (5) in Ref. 17] contains the integral

$$\int G(k_z - k'_z) F_n(k'_z) dk'_z e^{ik_z z} dk_z, \quad (4)$$

where  $k'_z$  and  $k_z$  are wave vectors limited to the first Brillouin zone of the bulk reference crystal (period =  $a$ ),  $F_n$  is an envelope function, and  $G$  is the composition modulation function defined in the Introduction. This integral can be reduced to

$$\begin{aligned} \int G(z') \tilde{F}_n(z') \tilde{\delta}(z - z') dz' &= G(z') \tilde{\tilde{F}}_n(z') \\ &\approx \tilde{G}(z') \tilde{F}_n(z'), \end{aligned} \quad (5)$$

where the tilde symbol represents the filtering out of all Fourier components outside the first Brillouin zone, the boundaries of which are at  $\pm k_{\text{BZ}}$ . The last step in Eq. (5) represents the standard convolution theorem in the limit  $k_{\text{BZ}} \rightarrow \infty$ . While this step should be a reasonable approximation for superlattices with layer thicknesses of more than a few monolayers, as in this work, it may be a poor approximation for a single monolayer, in which  $G(z)$  will contain large Fourier components close to the Brillouin zone boundary.

### III. CALCULATING THE ABSORPTION COEFFICIENT

The Fourier expansion method used to solve the superlattice Hamiltonian is discussed in Appendix A. Using this method, it is particularly simple to treat any of the TVK8 interface terms. The method is used to calculate the energy dispersions of the superlattice conduction and valence bands. In this Appendix, we also derive an expression for the oscillator strength of optical transitions between these bands. In this section, we present an efficient numerical approach for calculating the absorption coefficient of the superlattice, starting from the dispersion and oscillator strength results. We do not include excitonic effects in our treatment since the exciton binding energy is very small ( $\sim 2$  meV) and below our level of accuracy.

We divide  $k$ -space into many wedge-shaped cells,<sup>33</sup> using cylindrical polar coordinates. The joint density of states  $\rho$  for transitions between a given pair of bands is calculated by finding the number of transitions per unit energy interval within each cell,  $\rho = \frac{\Delta N}{\Delta E}$ , where  $\Delta N$  is proportional to the cell volume and  $\Delta E$  is the difference between the maximum and minimum energies at the eight cell corners. A fine enough resolution is selected in order to ensure sufficient accuracy. We have verified that the algorithm works well by comparing the result obtained with the analytical value calculated for the density of states of a very anisotropic parabolic dispersion, with masses  $m_1 = 5m_2 = 25m_3$ .

The absorption coefficient of a single cell  $\delta\alpha$ , with average transition energy  $E$ , joint density of states  $\rho$ , and average

oscillator strength  $S$ , is given by<sup>30</sup>

$$\delta\alpha(E)\Delta E = \frac{4\pi^2\alpha_{fs}\hbar^2}{n_{\text{act}}Em_0^2} \rho S f_v(\mathbf{k}) [1 - f_c(\mathbf{k})] \Delta E, \quad (6)$$

where  $\alpha_{fs}$  is the fine structure constant ( $\alpha_{fs} = \frac{e^2}{\hbar c} \approx \frac{1}{137}$ ),  $m_0$  is the free electron mass, and  $n_{\text{act}}$  is the refractive index of the material.  $f_v$  and  $f_c$  are the Fermi-Dirac functions of the valence and conduction band states, respectively. In order to create the full absorption spectrum, we can sum rectangle contributions with height  $\delta\alpha$  and width  $\Delta E$ , over all cells, centered around the mean transition energy for each cell, for all pairs of bands. However, it is more physically realistic to introduce inhomogeneous (Gaussian) broadening with a characteristic width  $\Delta E_{\text{in}}$ . Provided we choose cell dimensions small enough such that  $\Delta E < \Delta E_{\text{in}}$  in every cell, the result becomes insensitive to the number of cells used in the calculation. We therefore replace each rectangle by a Gaussian of the same area,  $\delta\alpha(E)\Delta E$ , centered at the average energy  $E$  and with a standard deviation  $\sigma = \frac{\Delta E_{\text{in}}}{2}$ . We use symmetry considerations to reduce the  $k$ -space grid to the minimum size. The calculation is performed only for positive  $q$  values and angles between 0 and  $\pi$ .<sup>34</sup> The result is then multiplied by 4.

## IV. EXPERIMENTAL METHODS

### A. Growth and characterization

The superlattice samples that were grown for this work had InSb-like interfaces. They were grown on 2- or 3-in GaSb substrates using a Veeco Gen III molecular beam epitaxy (MBE) machine, with group-III SUMO cells and group-V valved cracker cells.

X-ray diffraction (XRD) measurements were performed on a Bruker D8 Discover diffractometer. They were carried out to determine the superlattice period  $L$  and also the strain in the sample. We only used samples with an absolute lattice mismatch of less than 500 ppm, which corresponds to a separation of less than  $\pm 120$  arc seconds between the GaSb substrate peak and the zero-order superlattice peak (assuming no lattice relaxation in the superlattice). An example of the XRD measurements can be seen in Fig. 1. Very narrow satellite

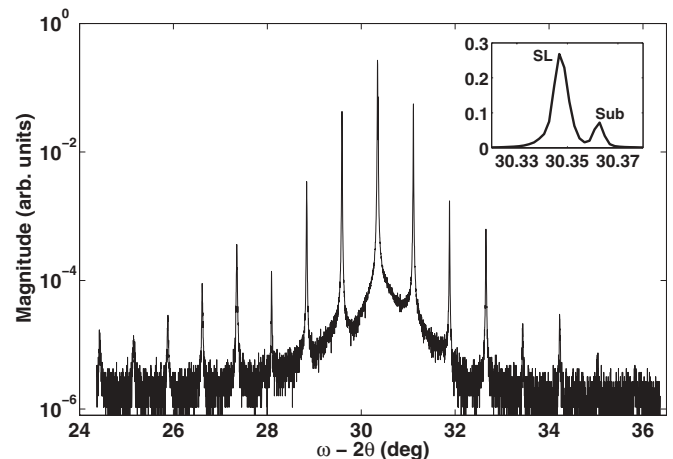


FIG. 1. Example of x-ray diffraction spectrum for a T2SL sample. Inset: Central peak region.

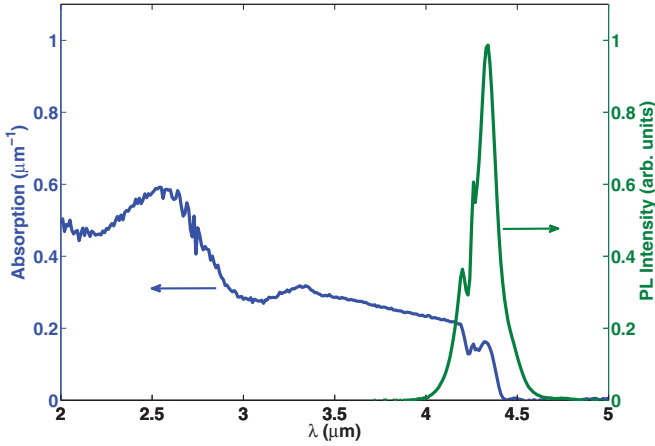


FIG. 2. (Color online) Normalized PL spectrum at 10 K and absorption spectrum at 77 K for sample SLMW02.

peaks can be observed, up to seventh order, indicating a very high quality of growth. The region close to the central peak is shown in the inset, and demonstrates the very small separation between the substrate peak and the zero-order superlattice peak, indicative of low strain as discussed above. Measurements of the superlattice period and central peak separation show very good uniformity from wafer center to wafer edge. The separation change from center to edge is typically less than 50 arc seconds, and the change in period is less than 1 Å.

Photoluminescence (PL) and absorption measurements were performed on a Bruker Equinox 55 Fourier Transform InfraRed (FTIR) spectrometer, with a resolution of  $4 \text{ cm}^{-1}$ . The PL was measured at 10 K and the absorption at 77 K, using a closed cycle Advanced Research Systems optical cryostat, and a liquid-nitrogen cooled optical test Dewar, respectively. For the absorption measurements, the transmission spectrum of the sample was measured before ( $T_1$ ), and after ( $T_2$ ), etching away part of the superlattice, to a depth of  $1\text{--}2 \text{ }\mu\text{m}$ . The absorption coefficient is then given by  $\alpha = \frac{1}{h} \ln(\frac{T_2}{T_1})$ , where  $h$  is the etch depth. This depth was measured with a Wyko interferometric microscope, which has nanometer-scale resolution in the vertical direction. In Fig. 2, we show examples of the PL and absorption spectra for sample SLMW02 (see Table I for details). It can be seen that the PL peak is very close to the onset wavelength of the absorption spectrum, showing that both techniques give a good estimate of the superlattice band gap at 77 K. The sharp features in both

TABLE I. List of the superlattices whose absorption spectra were used to determine the fitting parameters of the  $\mathbf{k} \cdot \mathbf{p}$  model. The table lists the measurement temperature of each spectrum and the layer widths of each superlattice, determined from growth flux measurements and adjusted by up to  $\pm 0.4 \text{ ML}$ .

Name	Temp. (K)	InAs (ML)	GaSb (ML)
SLMW01	77	8.7	10.6
SLMW02	77	8.6	13.5
SLMW03	300	8.7	15.7
SLLW01	77	14.4	7.2

spectra at  $4.2\text{--}4.3 \text{ }\mu\text{m}$  are due to atmospheric carbon dioxide absorption, and can be discounted.

### B. Experimental determination of the layer widths

We used an approach based on *in situ* beam-flux measurements of the In and Ga atomic beams to determine the individual InAs and GaSb layer widths in each superlattice. From these flux values, combined with the shutter timings, and the XRD measurement of the superlattice period, we have obtained a fairly accurate estimate of the layer widths. As will be shown below, the typical accuracy is  $\pm 0.25 \text{ ML}$ , with a maximum error of about  $\pm 0.4 \text{ ML}$ .

Our model of the superlattice growth is based on the usual assumption that the group-III atoms have high sticking coefficients and are therefore the species that determine the growth rate. The thickness of an InSb interface was included into the InAs layer width since both are determined by the In flux and it is assumed that the sticking coefficient does not change significantly between a bulk InAs layer and an InSb interface. Moreover, in order to achieve lattice matching, the InSb width has to be approximately 10% of the InAs width since the lattice mismatch between bulk InSb and the GaSb substrate is roughly 10 times greater than for bulk InAs. We can now write a simple equation for the total period of the  $i$ th sample as

$$1.1 \times (t_{\text{In}}\phi_{\text{In}})_i K_{\text{In}} + (t_{\text{Ga}}\phi_{\text{Ga}})_i K_{\text{Ga}} = L_i, \quad (7)$$

where  $t_{\text{In}}$  and  $t_{\text{Ga}}$  are the shutter times for InAs and GaSb layer growth, respectively,  $\phi_{\text{In}}$  and  $\phi_{\text{Ga}}$  are the In and Ga fluxes, and  $K_{\text{In}}$  and  $K_{\text{Ga}}$  are the growth coefficients that depend on the geometry of the MBE machine and the sample growth temperature.

Solving the system of equations

$$\begin{bmatrix} 1.1 \times (t_{\text{In}}\phi_{\text{In}})_1 & (t_{\text{Ga}}\phi_{\text{Ga}})_1 \\ 1.1 \times (t_{\text{In}}\phi_{\text{In}})_2 & (t_{\text{Ga}}\phi_{\text{Ga}})_2 \\ 1.1 \times (t_{\text{In}}\phi_{\text{In}})_3 & (t_{\text{Ga}}\phi_{\text{Ga}})_3 \\ \vdots & \vdots \\ 1.1 \times (t_{\text{In}}\phi_{\text{In}})_N & (t_{\text{Ga}}\phi_{\text{Ga}})_N \end{bmatrix} \begin{bmatrix} K_{\text{In}} \\ K_{\text{Ga}} \end{bmatrix} = \begin{bmatrix} L_1 \\ L_2 \\ L_3 \\ \vdots \\ L_N \end{bmatrix} \quad (8)$$

for  $N$  superlattices with different ratios of InAs to GaSb gives us the growth coefficients  $K_{\text{In}}$  and  $K_{\text{Ga}}$ . Over 30 samples were used in this fit, and a least-squares approach was used to determine values for the growth coefficients which gave the smallest error between the left- and right-hand sides of Eq. (8). The InAs width was then determined as  $L'_{\text{InAs}} = 1.05 \times t_{\text{In}}\phi_{\text{In}}K_{\text{In}}$  and the GaSb width as  $L'_{\text{GaSb}} = 0.05 \times t_{\text{In}}\phi_{\text{In}}K_{\text{In}} + t_{\text{Ga}}\phi_{\text{Ga}}K_{\text{Ga}}$ . Note that in this step the InSb layer is assumed to be divided equally between the InAs and GaSb layers. Since the period  $L$  has a higher accuracy than either of the widths determined using Eq. (8), the width of an InAs layer can be defined equally well as either  $L'_{\text{InAs}}$  or  $L - L'_{\text{GaSb}}$ , with corresponding expressions for a GaSb layer. We therefore take the average of the two expressions in order to obtain the most accurate width values:  $L_{\text{InAs}} = (L - L'_{\text{GaSb}} + L'_{\text{InAs}})/2$  and  $L_{\text{GaSb}} = (L - L'_{\text{InAs}} + L'_{\text{GaSb}})/2$  for InAs and GaSb, respectively. These values always add up to the most accurate period value  $L$  and are the values

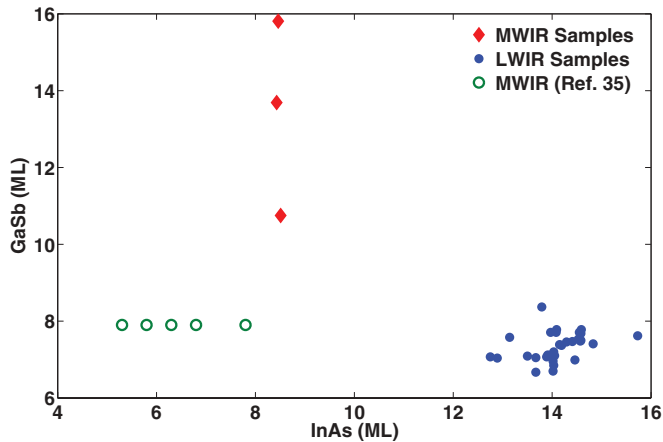


FIG. 3. (Color online) Superlattice layer widths used in the  $\mathbf{k} \cdot \mathbf{p}$  calculations. Solid: Layer widths determined from the flux measurements. Diamonds are for the MWIR and circles for the LWIR band-gap regions. Open circles: Nominal layer widths of the MWIR samples with InSb-like interfaces, taken from Ref. 35.

that we use in the  $\mathbf{k} \cdot \mathbf{p}$  calculations discussed in the next section.

The results of the layer-width fitting by the flux method are shown graphically in Fig. 3, where the solid points show  $L_{\text{GaSb}}$  plotted against  $L_{\text{InAs}}$ . The points fall into distinct groups: the three samples with an InAs width of between 8 and 9 ML are plotted as solid diamonds and have band-gap wavelengths in the mid-wave-infrared (MWIR) atmospheric transmission window (3–5  $\mu\text{m}$ ), while those with InAs widths of between 12 and 16 ML are plotted as solid circles and have band-gap wavelengths in the long-wave-infrared (LWIR) atmospheric transmission window (8–12  $\mu\text{m}$ ). Note that in growing the three MWIR samples, the InAs widths were intentionally kept the same, while the GaSb width was varied by 2 to 3 ML in each direction. The fitted values agree very well with a constant value for the InAs width, and with the intended changes to the GaSb layer. The five open circles are nominal width values for five MWIR samples with InSb-like interfaces described in Ref. 35. They have been included in Fig. 3 because we compare their band-gap wavelengths with those of our own samples in Sec. V.

The calculated period  $L'_{\text{InAs}} + L'_{\text{GaSb}}$  had an error of less than 1.5  $\text{\AA}$ , compared with the XRD period value, in more than 80% of the samples. The maximum error was 2.4  $\text{\AA}$ . This corresponds to a typical error in the period of 0.5 ML, and a maximum error of 0.8. If we assume that the errors in the flux widths  $L'_{\text{InAs}}$  and  $L'_{\text{GaSb}}$  are similar and uncorrelated, and significantly larger than the error in the XRD period  $L$ , then the error in the expression  $L - L'_{\text{GaSb}} + L'_{\text{InAs}}$  will be the same as the error already determined for  $L'_{\text{InAs}} + L'_{\text{GaSb}}$ . Thus, the error in the individual InAs layer width  $L_{\text{InAs}} = (L - L'_{\text{GaSb}} + L'_{\text{InAs}})/2$  will be half as much, with a maximum value close to 0.4 ML. This value represents the experimental uncertainty with which we can compare our theoretical model with experimental results. As will be shown in the next section for a set of more than 30 samples, it agrees quite well with the statistical distribution of the difference  $\Delta L_{\text{InAs}}$  between the InAs layer width  $L_{\text{InAs}}$ , determined as above, and the InAs layer width calculated by fitting our  $\mathbf{k} \cdot \mathbf{p}$

model to the measured XRD period and photoluminescence band-gap wavelength. This distribution has a maximum width of  $\pm 0.4$  ML and a standard deviation of about 0.2 ML. As mentioned in Sec. II, these values justify the inclusion in this work of terms of order  $\ell = 1$ , while omitting those with  $\ell \geq 2$ .

## V. RESULTS

In this section, we demonstrate that it is possible to fit our experimental band-gap data with a single set of 6 fitting parameters, for more than 30 superlattice samples spanning the wavelength range 4.3 to 12  $\mu\text{m}$ . The fitting parameters are three interface parameters  $D_S$ ,  $D_X$ , and  $D_Z$ , two Luttinger parameters  $\gamma_1$  and  $\gamma_2$  for InAs, and the valence band offset. In Appendix C, it is shown that the other Luttinger parameters are not independent but can be derived from the two fitted ones. We do not rely on the literature values of the Luttinger parameters because there is quite a wide variation of quoted values (e.g., see Ref. 36 which gives typical ranges) and because the source of the most widely used values<sup>29</sup> is based on theoretical scaling arguments rather than precise experimental determinations. In addition, we find that our results are quite sensitive to even small changes in some of their values. All other model parameters are well established, either from x-ray measurements (lattice parameter), spectroscopic measurements (band gaps, conduction band effective mass, deformation potentials), or mechanical measurements (compliance coefficients), and are taken from the databases in Refs. 27 and 28. Special mention should be made of the values we have used for the  $\mathbf{k} \cdot \mathbf{p}$  parameter  $E_P$  in InAs and GaSb. Our values differ from some of those used by other workers, and are based on a fit to bulk band gap and conduction band mass data from the same database sources.<sup>37</sup> The fitting procedure uses a bulk five-band  $\mathbf{k} \cdot \mathbf{p}$  model, as discussed in Appendix C, and gives values which are very close to those quoted by Lawaetz.<sup>29</sup> Table II in Appendix B lists our  $E_P$  values, and the values of all the parameters taken from literature databases. The final values of the fitted parameters are listed in Table III of the same Appendix. In that table, we quote values of 0.2 eV  $\text{\AA}$  for both interface parameters  $\alpha$  and  $\beta$ . Nonzero values were chosen for our calculations in order to demonstrate a spin splitting in the valence band dispersion, as shown in Fig. 4. However, zero values can be used with negligible effect on the modeled band gaps or absorption spectra, so these are not considered to be real fitting parameters. Their small values are consistent with the theoretical predictions of Sec. II. An additional fitting parameter  $\eta$  is required to fit the model to experimental absorption spectra. This parameter simply scales the absolute value of the modeled absorption, as discussed in Appendix A, but does not affect the band gaps or the wavelengths of any spectral features. We use a value of 1.45 in all of the examples discussed in the following.

We begin by discussing the general form of the dispersion relation in Sec. V A and the absorption spectrum in Sec. V B. For the absorption spectrum, we show that it is important to use an energy-dependent inhomogeneous broadening parameter in the model in order to obtain a true likeness to the measured spectrum. We then present a detailed comparison between

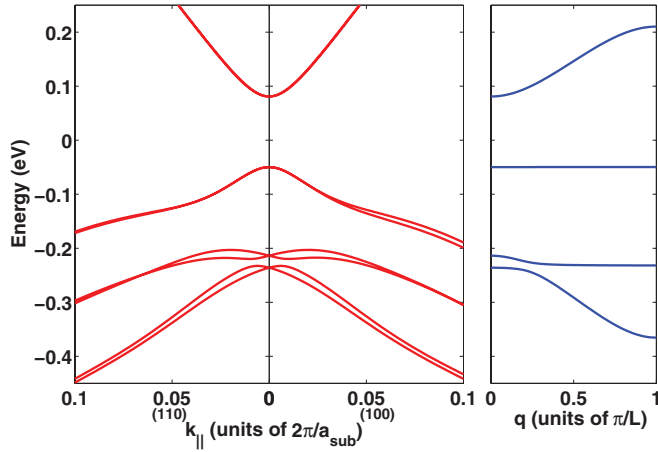


FIG. 4. (Color online) Dispersion relation of a 13.8/7.8 InAs/GaSb T2SL with InSb interfaces (superlattice period = 21.6 ML) for several directions in the Brillouin zone.

modeled and experimental results in Sec. VC, for both absorption spectra and band-gap measurements.

### A. Dispersion relation

The calculated dispersion relation of a 13.8/7.8 T2SL is shown in Fig. 4 for two in-plane directions in the Brillouin zone, and the perpendicular (growth) direction. This combination of layer widths was selected because its fundamental band gap corresponds to  $\lambda_0 = 9.5 \mu\text{m}$ , which is a useful wavelength for infrared detection in the LWIR atmospheric window.

As seen in the figure, there is a spin splitting in the in-plane direction, along with a small shift of the maximum energy of each spin band away from the Brillouin zone center. This occurs when the  $\alpha$  parameter is nonzero and is related to the orthogonal nature of the In-Sb bonds at the two interface planes of a superlattice period.

### B. Absorption spectrum

As mentioned in Sec. III, the  $k$ -space grid has to be dense enough to ensure that the energy difference obeys the relation  $\Delta E < \Delta E_{\text{in}}$ . In short-period superlattices, we expect that the dominant mechanism that determines  $\Delta E_{\text{in}}$  will be fluctuations in the layer widths. In a simple quantum well, fluctuations of the well width cause energy-level broadening by an amount roughly proportional to the confinement energy. We have therefore chosen to represent the inhomogeneous broadening by a formula which gives an increasing level of broadening with increasing transition energy (or shorter transition wavelength  $\lambda$ ):

$$\Delta E_{\text{in}} = \Delta E_0 + \frac{\Delta E_1 - \Delta E_0}{\lambda_0 - \lambda_1} (\lambda_0 - \lambda), \quad (9)$$

where  $\Delta E_1$  and  $\Delta E_0$  ( $< \Delta E_1$ ) are the broadening at wavelengths  $\lambda_1$  and  $\lambda_0$  ( $> \lambda_1$ ), respectively.

A typical spectrum contains two main features. One is the band-gap energy, labeled  $E_0$ . The other is a peak at a higher energy, labeled  $E_D$ , which corresponds to the transition between the second heavy-hole band (HH2) and the first conduction band (E1), at the edge of the growth direction

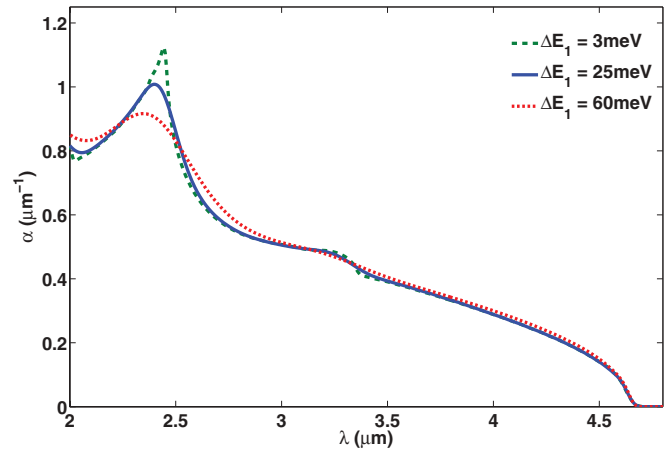


FIG. 5. (Color online) Calculated absorption spectrum for sample SLMW01 with  $\Delta E_0 = 3 \text{ meV}$ , and with three different values of  $\Delta E_1$ : 3, 25, and 60 meV.

Brillouin zone. It is convenient to set  $\lambda_1$  and  $\lambda_0$  at these energies ( $\lambda_1$  for  $E_D$  and  $\lambda_0$  for  $E_0$ ), using the relation  $\lambda = \frac{hc}{E}$ .  $\Delta E_0$  is expected to be of the order of the PL line width and  $\Delta E_1$  is determined empirically to give the best fit to the shape and amplitude of the  $E_D$  peak in a measured absorption spectrum. Figure 5 shows the calculated 77-K absorption spectrum of sample SLMW01 (for sample details, see Table I) with three values of  $\Delta E_1$ : 3, 25, and 60 meV, while  $\Delta E_0$  remained constant at 3 meV. The calculation parameters can be found in Appendix B and are based on a fitting procedure described in the next section. For the time being, we simply note the differences in the spectrum when changing the inhomogeneous broadening. In all three calculations,  $\lambda_1 = 2.3 \mu\text{m}$  and  $\lambda_0 = 4.6 \mu\text{m}$ . In addition, the  $k$ -space grid was chosen to be dense enough, so that the condition  $\Delta E < \Delta E_{\text{in}}(\lambda)$  was maintained over the whole spectral region, except for the case of  $\Delta E_1 = 3 \text{ meV}$ , where it was maintained over most of the region. It can be seen that in the case where all broadening is equal to the band-gap broadening (dashed line), the spectrum looks unphysical and the  $E_D$  peak is too sharp and almost singular. On the other hand, increasing the broadening too much can result in over broadening, which causes other features in the plot to vanish (dotted line). The solid line ( $\Delta E_1 = 25 \text{ meV}$ ) corresponds to a more realistic value for  $\Delta E_1$  and this is the value that was used to fit the absorption spectra in our three MWIR samples. For the absorption spectrum of our LWIR sample, SLLW01, larger values had to be used for both broadening energies  $\Delta E_0 = 15 \text{ meV}$  and  $\Delta E_1 = 60 \text{ meV}$ , with  $\lambda_1 = 2 \mu\text{m}$ . The reason for this increase is that a substrate was selected which had transmission in the LWIR range, and unfortunately this substrate was of poorer quality than those used for the growth of our other samples. The surface of the grown wafer was significantly rougher than for the superlattices that were used for the MWIR absorption measurements.

We have found that it is possible to decrease the number of points in the  $k$ -space grid considerably, even to the point where the condition  $\Delta E < \Delta E_{\text{in}}(\lambda)$  no longer applies for all transitions, before the form of the absorption spectrum starts to show significant deviations. In our experience, it is crucial to

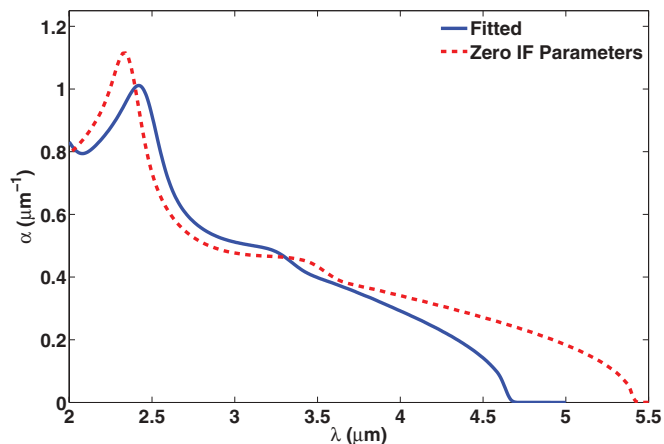


FIG. 6. (Color online) Calculated absorption spectrum of sample SLMW01 with fitted (solid) and zero (dashed) interface parameters.

maintain the condition  $\Delta E < \Delta E_{\text{in}}(\lambda)$  for transitions near the absorption edge, while some transitions at higher energies, including  $E_D$ , can have  $\Delta E > \Delta E_{\text{in}}$ . Thus, we find that when integrating over 10% of the in-plane Brillouin zone, a reasonable number of points in  $k$ -space is 50 values of the in-plane wave vector  $K$ , 5 values of the in-plane polar angle  $\theta$ , and 20 values of the growth direction wave vector  $q_z$ . This is enough to obtain an absorption plot that is indistinguishable from a plot like the solid line shown in Fig. 5, where all transitions comply with the condition  $\Delta E < \Delta E_{\text{in}}(\lambda)$ . It means that we can reduce the running time of the calculation considerably because we only have 5000  $k$ -space points (this is about 20% of the number of points used to calculate the plots in Fig. 5). We have managed to reduce the calculation time for one spectrum of a typical T2SL to between two and four minutes, using a MATLAB program optimized for parallel computing, on a desktop computer with a consumer level quad-core processor.

Finally, we demonstrate the significance of the interface parameters  $D_S$ ,  $D_X$ , and  $D_Z$  on the calculated absorption spectrum. Figure 6 compares the absorption spectra of sample SLMW01 when calculated with the fitted or zero interface parameters. The latter corresponds to a model without an interface matrix (if we ignore the negligible effect of  $\alpha$  and

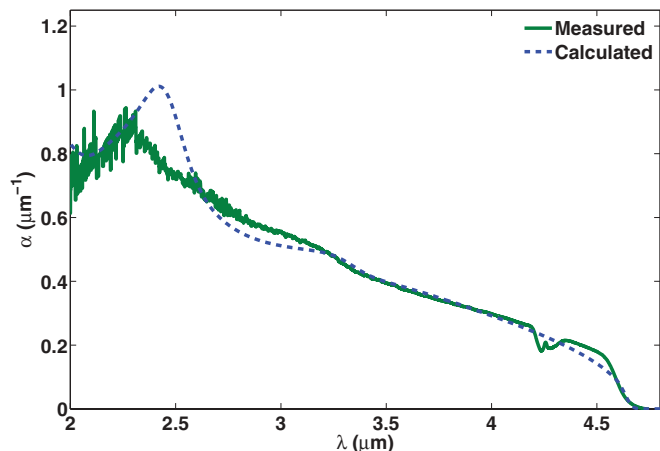


FIG. 7. (Color online) Measured (solid line) and calculated (dashed line) absorption spectrum of sample SLMW01, at 77 K.

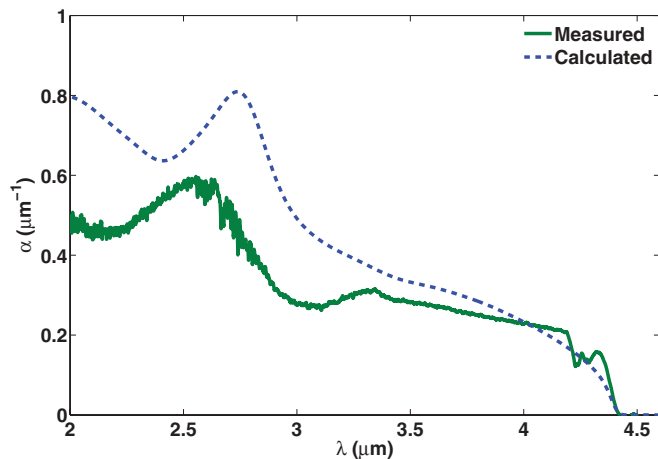


FIG. 8. (Color online) Measured (solid line) and calculated (dashed line) absorption spectrum of sample SLMW02, at 77 K.

$\beta$ ). As seen in the figure, the interface parameters have a substantial effect. Every feature in the spectrum, especially the cutoff wavelength, is shifted and not in the correct place if zero values are used. If we try to fit the superlattice layer widths with zero interface parameter values, we get a very large deviation from the flux-calculated widths ( $> 1$  ML), well beyond the acceptable error discussed in Sec. IV.

### C. Fit to experimental results

We first compare the calculated absorption spectra of four representative superlattice samples with their measured spectra, as shown in Figs. 7–10. Three of these are in the MWIR spectral region and one in the LWIR region. For two of the MWIR samples, and the LWIR sample, the fits are shown for spectra measured at 77 K, while for the third MWIR sample, the fit is shown for a 300-K spectrum. The four samples are listed in Table I together with the temperature at which each of the presented absorption spectra was measured. Although we only show a fitted room-temperature spectrum for sample SLMW03, we have obtained similar quality fits for the other two MWIR samples at room temperature. We did not measure the absorption spectrum of this sample at 77 K.

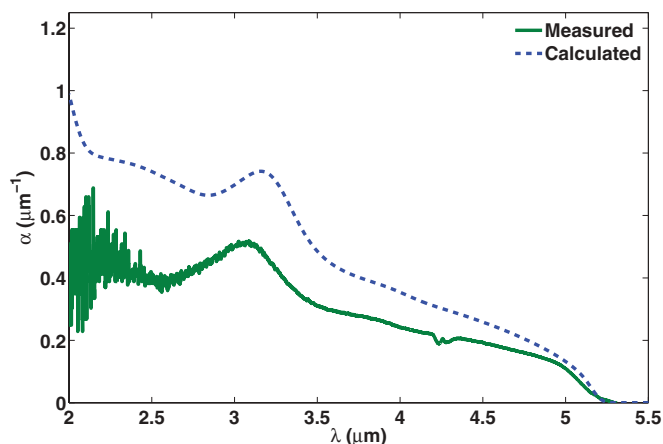


FIG. 9. (Color online) Measured (solid line) and calculated (dashed line) absorption spectrum of sample SLMW03, at 300 K.

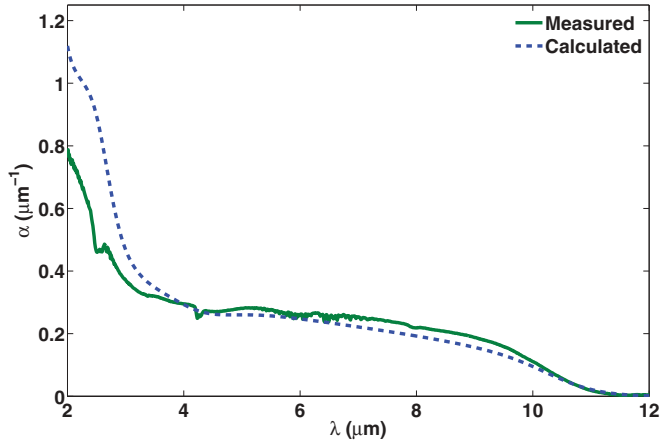


FIG. 10. (Color online) Measured (solid line) and calculated (dashed line) absorption spectrum of sample SLLW01, at 77 K.

During the fitting process, great effort was made to fit both the band-gap energy  $E_0$  and the peak energy  $E_D$  in the absorption spectrum. We allowed changes of up to  $\pm 0.4$  ML in the InAs widths (at constant period), relative to the values determined experimentally from the beam-flux measurements, consistent with the precision of the beam-flux measurements discussed above. In all cases, a much smaller change was needed in order to find the best match to the measured band-gap wavelengths. The final width values are also listed in Table I.

After the optimal set of parameters was found from the four absorption spectra, the same parameter set was used to calculate the PL peak wavelengths (band-gap wavelengths) of many other samples. The experimental layer widths were used without adjustment. The solid points in Fig. 11 show the deviation between the calculated and measured wavelengths for our samples ( $\Delta\lambda = \lambda_{\text{PL}} - \lambda_{\mathbf{k}\cdot\mathbf{p}}$ ). All samples are within a  $0.6\text{-}\mu\text{m}$  wavelength deviation from the measurement, and most have a deviation of less than  $0.4\ \mu\text{m}$ . The value of the valence band offset (VBO) that was used ( $0.560\ \text{eV}$ ), both to fit the low-temperature absorption spectra and to predict the PL wavelengths, was found (iteratively) by ensuring that the wavelength deviations in Fig. 11 had a fairly symmet-

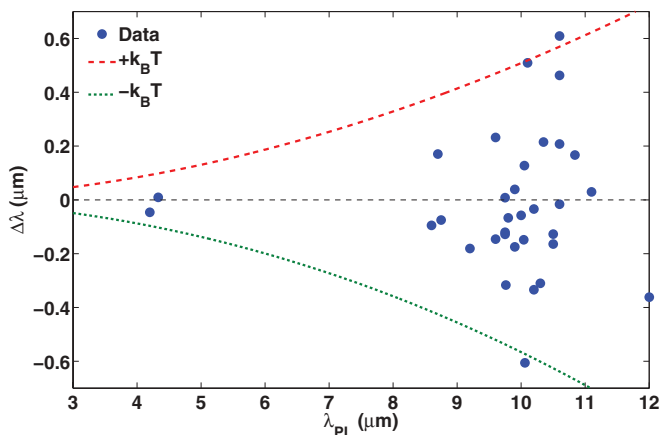


FIG. 11. (Color online) Deviation of predicted PL wavelengths from the measured PL peak wavelengths. The dashed and dotted lines indicate the effect of an error of  $k_B T$  in band-gap energy at 77 K.

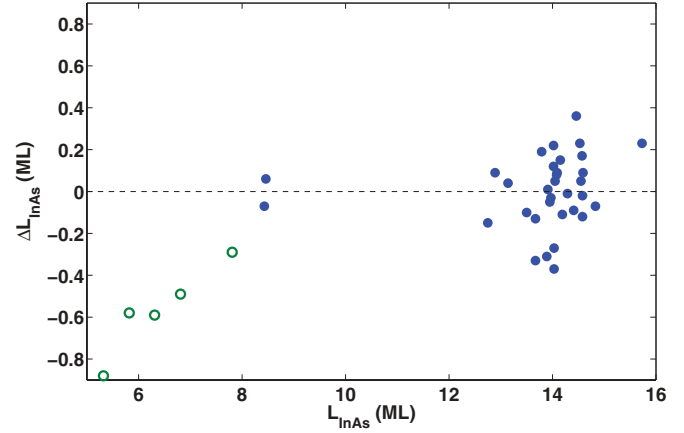


FIG. 12. (Color online) Deviation of fitted InAs widths from the growth nominal widths. Solid: Nominal width is the width calculated by the flux method. Circles: Nominal layer width is taken from Table VI in Ref. 35.

rical distribution around zero, with no systematic bias. It corresponds to a band overlap in the unstrained materials of  $0.142\ \text{eV}$ .

The dashed and dotted lines in Fig. 11 indicate the range of error for a variation of  $\pm k_B T$  in the band-gap energy at 77 K. Since one of the main applications of InAs/GaSb superlattices is as the absorber in an infrared detector operating typically at 77 K, the fact that all the points lie within these lines shows that the wavelength deviations are mostly below typical thermal broadening. The precision of our results is also shown in Fig. 12, in this case in terms of the layer-width uncertainty. The solid points in Fig. 12 show a comparison between the InAs layer width determined by a fit to the measured PL peak wavelength and XRD period,  $L_{\text{InAs},\mathbf{k}\cdot\mathbf{p}}$ , and that determined by the flux method,  $L_{\text{InAs}}$ , for all of our samples. In the figure, the difference between these two values,  $\Delta L_{\text{InAs}} = L_{\text{InAs}} - L_{\text{InAs},\mathbf{k}\cdot\mathbf{p}}$ , is plotted as a function of  $L_{\text{InAs}}$ . All of our samples fit within the allowed experimental margin of error of  $\pm 0.4$  ML discussed in Sec. IV. Indeed, more than 70% of them fall within a range of  $\pm 0.2$  ML, which is close to the standard deviation of the distribution of  $\Delta L_{\text{InAs}}$  values in Fig. 12.

We have also included data in Fig. 12 as open points, for five MWIR samples with InSb-like interfaces and with band-gap wavelengths between  $3.5\text{--}4.5\ \mu\text{m}$ , taken from Szmulowicz, Haugan, and Brown,<sup>35</sup> where the experimental layer widths used for  $L_{\text{InAs}}$  are their quoted nominal values. In this case, the deviations are larger than for our samples, with the width deviation increasing as the InAs layer width decreases. Most of the InAs width deviations for the five samples are between  $0.2$  and  $0.6$  ML, and the largest is still less than  $0.9$  ML. We take this behavior to indicate reasonable agreement with our model, noting that the layer widths in that work were standard nominal values and may not have been calibrated as precisely as in this work.

## VI. DISCUSSION

The optical absorption and photoluminescence results presented in Figs. 7–12 of the previous section show that our  $\mathbf{k} \cdot \mathbf{p}$  model provides a reasonably good description of the main spectral features of InAs/GaSb superlattices with InSb-like

interfaces, over a wide range of band-gap energies. The band gap  $E_0$  and the peak  $E_D$  in the absorption spectra are reproduced quite well, both in energy and form. In addition, an interesting blue-shift effect is demonstrated in Figs. 7 and 8, which show a shift of nearly  $0.3 \mu\text{m}$  when the GaSb width is increased by  $\sim 3$  ML without changing the InAs width. Figure 12 shows that the shift can be fitted with a precision of better than 0.1 ML. Thus, the blue-shift is also reproduced very well by our model and is an effect that some previous  $\mathbf{k} \cdot \mathbf{p}$  treatments have failed to predict.<sup>26</sup> In the remainder of this section, we discuss a number of issues concerned with the accuracy of our treatment and how it compares with other recent work.

The main source of error in our comparison between modeled and experimental results is an imprecise knowledge of the layer widths, which are known with an individual uncertainty of about  $\pm 0.4$  ML, or with a statistical uncertainty of about  $\pm 0.2$  ML for our sample set. We can compare this uncertainty with the effect of some of the second-order terms, of magnitude  $\ell = 2$ , that we have omitted, namely, the off-diagonal term  $h_{SZ} = \sum_i \delta(z - z_i) i \chi_1 k_z$  and its Hermitian conjugate  $h_{ZS} = -\sum_i i \chi_1 k_z \delta(z - z_i)$ , which appear in Eqs. (28) and (30) of Ref. 17. Taking a characteristic value of  $\chi_1 = 3 \text{ eV \AA}^2$ , based on our best estimate of the momentum, band gap, and interface parameters on which this coefficient is based, we calculate a shift in the band gap of the superlattice shown in Fig. 4 equivalent to an InAs width change (at constant period) of less than 0.3 ML. This is comparable with our experimental accuracy limit and so justifies our omission of such terms.

In our solution of the Hamiltonian given by Eqs. (1)–(3), described fully in Appendix A, we do not include Fourier components for the envelope functions outside the first Brillouin zone [i.e.,  $j \leq j_{\text{max}}$  in Eq. (A2)]. We now consider how this may affect the accuracy of our approach compared with other approaches, in particular exact real-space solutions based, for example, on transfer-matrix techniques.<sup>35</sup> The exact solution can be found in our case by increasing the limits of the summation in Eq. (A2) beyond the value of  $j_{\text{max}}$  given in Eq. (A3b) until the band-edge energies converge fully. We have found that for representative superlattices with band-gap wavelengths between  $3.5$  and  $12 \mu\text{m}$ , the difference between these energies and those for  $j \leq j_{\text{max}}$  corresponds to InAs width changes of less than  $+0.3$  ML for the conduction band, and about  $-0.5$  ML for the valence band (at constant period). Moreover, for two superlattices with the same period and band gap, calculated with a truncated or a full Fourier summation, there can be a difference of up to  $0.6$  ML in the InAs thickness. The parameters which give the best fit to experimental data for an exact real-space solution will therefore differ quite noticeably from those given in Table III of Appendix B for our truncated solution. We have not checked whether a unique set of parameters can be found in that case which gives the same quality of fit to the data. It should be noted, however, that the truncated solution better reflects the Fourier makeup of the true envelope functions, which contain no components outside the first Brillouin zone. Nevertheless, this solution, or an exact real-space solution, are both approximations. As discussed at the beginning of Appendix A, the exact solution

must be obtained by solving the  $k$ -space Hamiltonian which contains none of the approximations required to transform it to real space. Fortunately, these approximations are expected to introduce errors corresponding to  $\ell \geq 2$  (see Appendix A) which are small enough to be ignored at our stated level of accuracy, and also appear to be consistent with variations between the different real-space treatments estimated above.

Two  $\mathbf{k} \cdot \mathbf{p}$  treatments which drew attention to the significance of interface effects in InAs/GaSb superlattices are those of Lau and Flatte<sup>38</sup> in 2002, and Szmulowicz, Haugan, and Brown<sup>35</sup> in 2004. The experimental results of the latter work for samples with InSb-like interfaces were included in Fig. 12 above (see Sec. V). Both works considered short-period superlattice samples with band-gap wavelengths in the range  $3$ – $4.5 \mu\text{m}$ . In the work of Lau and Flatte, on mixed interface samples, limited agreement was obtained between experimental band-gap and absorption results, while Szmulowicz *et al.* reported reasonable agreement of band-gap energies for samples with either identical or mixed interfaces. Szmulowicz *et al.* used  $\alpha$  values of  $\alpha_{\text{InSb}} \approx 3.5 \text{ eV \AA}$  and  $\alpha_{\text{GaAs}} \approx 0 \text{ eV \AA}$  to model InSb-like and GaAs-like interfaces, respectively, while diagonal interface parameters  $D_S$ ,  $D_X$ , and  $D_Z$  were not included (Lau and Flatte used an identical approach to Szmulowicz *et al.*, with  $\alpha_{\text{InSb}} \approx 2.6 \text{ eV \AA}$  and  $\alpha_{\text{GaAs}} \approx 0.4 \text{ eV \AA}$ ). Most other model parameters in Szmulowicz *et al.* are similar to the parameters listed in Appendix B of this work, although our value of  $E_P$  for GaSb (discussed in Appendix B) is  $\sim 3 \text{ eV}$  smaller, which is quite a significant difference. The agreement between experimental and theoretical results in both their work and our work highlights the potential ambiguity of  $\mathbf{k} \cdot \mathbf{p}$  treatments, where good agreement with band-gap data can be obtained over a limited range of wavelengths for different parameter sets. This ambiguity must be resolved by fitting additional features, such as  $E_D$ , and increasing the wavelength range. In fact, using  $\alpha$  values close to  $3.5 \text{ eV \AA}$  for InSb-like interfaces and setting all other interface parameters to zero, as in Ref. 35, we were unable to obtain a reasonable fit to the band gap  $E_0$  or the higher-energy  $E_D$  feature in our measured absorption spectra shown in Figs. 7 and 8 for SLMW01 and SLMW02.

The ability of our parameter set to fit experimental data with band-gap wavelengths between  $3.5$  and  $12 \mu\text{m}$  and to provide a reasonably accurate prediction of the form and energy of the  $E_D$  feature for superlattices with band-gap wavelengths in both the MWIR and LWIR ranges gives us some confidence in the validity of our approach. In this approach, the only significant interface contribution is from the three  $D$  parameters, while the  $\alpha$ - and  $\beta$ -interface parameters are essentially negligible. Our approach is consistent with the expectation, mentioned earlier, of much smaller values for  $\alpha$  and  $\beta$  than for the  $D$  parameters in no common atom superlattices. It is interesting to note that we have succeeded in using a single set of interface parameters for nearly 40 superlattice samples with InSb-like interfaces, including those of Ref. 35, grown at different times and even in two different laboratories (see Fig. 12). This suggests that these interface parameters are not very sensitive to variations in interface abruptness. A possible reason is given by the following argument. Although the functions  $\Phi_0^s$  and  $\Phi_0^v$  in the TVK8 model (see Sec. II) reduce in amplitude as the interface abruptness is reduced,<sup>17</sup> this reduction is not related

to interface grading where, for example, the In-Sb interface bonds are distributed over several ML. The TVK8 model only applies to metallurgically abrupt interfaces, located on a single atomic plane. Foreman<sup>39</sup> has pointed out that when the interfaces become significantly graded, an atomic description must be used. Using such an approach, Foreman has shown that the interface band mixing is actually rather insensitive to a reduction in interface abruptness: its strength remains essentially constant and only its width changes.

A nonzero interface parameter  $\alpha$  causes the mixing of heavy and light holes at the zone center. This can introduce a contribution to the anisotropy of the optical and electrical properties for samples in which the symmetry along the growth direction is broken,<sup>14–16</sup> for example, when alternating InSb- and GaAs-like interfaces are used, or when interfaces of the same type are used and an electric field is applied perpendicular to the layers. Semenikhin *et al.*<sup>40</sup> calculated a value of  $\alpha = 0.23 \text{ eV \AA}$  for a planar abrupt InAs/GaSb interface<sup>41</sup> using a pseudopotential approach similar to that introduced by Foreman.<sup>8</sup> They showed that for such a small value of  $\alpha$ , other contributions to the optical anisotropy, such as those due to bulk inversion asymmetry and relativistic effects, are larger than the nonrelativistic  $\alpha$ -interface contribution.<sup>42</sup> On the other hand,  $\alpha$  values greater than  $3 \text{ eV \AA}$  should result in quite dramatic optical anisotropies. Our results, in which  $\alpha \approx 0$ ,  $\beta \approx 0$ , are consistent with the estimate of Semenikhin *et al.*<sup>40</sup> and suggest that anisotropy effects will be very weak. Experimental investigations of the strength of the optical anisotropy for polarizations along [110] and  $[\bar{1}10]$  could therefore be useful for confirming the magnitude of  $\alpha$ , and may help to provide an independent estimation of its magnitude.

A number of other  $\mathbf{k} \cdot \mathbf{p}$  treatments have recently claimed good correspondence between the modeled and measured band gaps. Li *et al.*<sup>43</sup> use an interface matrix in which  $D_S = \beta = 0$  and  $\alpha = D_X = D_Z = 0.870 \text{ eV} \times 6.1 \text{ \AA} \approx 5.3 \text{ eV \AA}$  for InAs on GaSb (GaAs like interface) and  $0.49 \text{ eV} \times 6.1 \text{ \AA} \approx 3.0 \text{ eV \AA}$  for GaSb on InAs (InSb-like interface). They studied superlattices with band-gap wavelengths in the range of  $\sim 3.5$  to  $5 \mu\text{m}$ . Hong *et al.*<sup>44</sup> worked over a similar wavelength range and used a standard piecewise  $\mathbf{k} \cdot \mathbf{p}$  model with no interface terms. They claimed good correspondence with experimentally measured band-gap wavelengths when the interfaces were graded over about 2 ML and the superlattice had the composition  $\text{InAs}_{0.91}\text{Sb}_{0.09}/\text{GaSb}$ . This further highlights the ambiguity of different parameter sets and interface formulations for a narrow range of band-gap wavelengths. Neither of these approaches treats the interfaces consistently with the TVK8 model, which we believe to have a stronger physical basis.

## VII. CONCLUSIONS

The eight-band TVK8  $\mathbf{k} \cdot \mathbf{p}$  Hamiltonian has recently been proposed<sup>17</sup> as a successor to the Burt-Foreman model of semiconductor superlattices. It includes all important bulk and interface terms up to order  $\ell = 2$  in  $\delta\bar{V}(\bar{\mathbf{k}}a)^\ell$ , including some terms that were left out in the Burt treatment. This results in different symmetrization expressions for the bulk terms compared with the Burt-Foreman model, and it introduces important diagonal interface terms for no common atom superlattices, such as InAs/GaSb, that are absent in ideal common atom superlattices, such as GaAs/AlAs.

We have used a model based on the TVK8 Hamiltonian to fit the absorption spectra of representative InAs/GaSb superlattices measured at 77 and 300 K, with band-gap wavelengths in the technologically useful 3–5 and 8–12  $\mu\text{m}$  ranges, corresponding to important transmission windows in the atmosphere. Our model only includes the Fourier components of the envelope functions lying in the first bulk Brillouin zone, and is able to reproduce all of the main features of the absorption spectra reasonably well, including the blue-shift of the band-gap wavelength with increasing GaSb thickness and a strong peak arising from zone boundary transitions between the second heavy-hole state and the first electron state. The same model was also able to predict the band-gap wavelengths of about 30 more superlattice structures, with a typical accuracy of  $\pm 0.3 \mu\text{m}$ . These wavelengths were measured by photoluminescence spectroscopy at 10 K and spanned a range similar to the band-gap wavelength range of the absorption measurements. If the measured photoluminescence wavelength is used to predict the layer widths, the typical deviation from the measured value is 0.2 ML with a maximum error of 0.4 ML. This error agrees very well with the error in the layer widths calculated from the reactor growth rate constants, and represents the typical precision with which an InAs/GaSb superlattice structure can be grown.

A ML change in layer width corresponds to a band-edge energy shift of order  $\delta\bar{V}(\bar{\mathbf{k}}a)$ . Our individual layer-width accuracy of  $\pm 0.4$  ML means that the layer widths of nominally identical superlattices may differ by up to 0.8 ML. Therefore, the fluctuation in the individual band-gap energies will also be of order  $\delta\bar{V}(\bar{\mathbf{k}}a)$ . However, since we consider the statistical distribution of more than 30 superlattices, the center of the distribution can be determined rather more accurately, to within one or two tenths of a monolayer, and on this basis we have justified keeping terms in the TVK8 Hamiltonian with  $\ell = 1$ , while omitting all those with  $\ell > 1$ . This essentially reduces the number of unknown fitting parameters to six: two Luttinger parameters, three interface parameters, and the valence band offset. All other  $\mathbf{k} \cdot \mathbf{p}$  parameters can be determined with reasonable accuracy from available experimental x-ray, spectroscopic, and mechanical data. We have demonstrated that, at the stated level of accuracy, the remaining four Luttinger parameters are not independent and can be determined from the two independent ones and measured band-gap energies in bulk InAs and GaSb. Our full set of Luttinger parameters is close to the set predicted by Lawaetz,<sup>29</sup> with a maximum deviation in any parameter of 0.6. The diagonal interface parameters have fitted values of  $D_S = 3 \text{ eV \AA}$ ,  $D_X = 1.3 \text{ eV \AA}$ , and  $D_Z = 1.1 \text{ eV \AA}$  at 77 K. The off-diagonal interface parameters  $\alpha$  and  $\beta$  are too small to be fitted with any accuracy and have negligible effect on the unpolarized absorption spectra. Measurements of the absorption difference between [110] and  $[\bar{1}10]$  polarizations in asymmetric structures, or in the presence of a perpendicular electric field, may help to establish a more precise value for  $\alpha$ . Our fitted value of the band overlap between unstrained InAs and unstrained GaSb is 0.142 eV. Note, however, that since our treatment has a typical error corresponding to  $\ell = 2$  because terms of this order have been omitted, the accuracy of the fitted overlap can be no better than about  $\pm 0.01 \text{ eV}$ .<sup>45</sup> We have also proposed values for the room-temperature Luttinger

and interface parameters by fitting the TVK8 model to room-temperature absorption spectra with band-gap wavelengths of about  $5 \mu\text{m}$ .

We suggest that our method of reducing the number of independent Luttinger parameters should provide a useful approach for the determination of the Luttinger parameters in narrow band-gap semiconductor alloys such as InAsSb, where there is a significant degree of band-gap bowing. Using the constraint relations given in Eqs. (C1a)–(C1d) and band-gap results from spectroscopic measurements,  $\gamma_3$  for the alloy and the Luttinger parameters of a reference material such as GaAs can be calculated by adjusting  $\gamma_1$  and  $\gamma_2$  for the alloy until the error in the three GaAs Luttinger parameter values is minimized.

## ACKNOWLEDGMENTS

The authors would like to acknowledge useful discussions with Y. Rosenwacks of the Department of Physical Electronics, Tel Aviv University. P.C.K. acknowledges useful correspondence with É. E. Takhtamirov. We also thank M. Katz and O. Westreich of the Soreq Research Center for assistance with some of the PL measurements.

## APPENDIX A: METHOD OF SOLUTION

### 1. Fourier-transformed Hamiltonian

We have followed the work of Gershoni *et al.*<sup>30</sup> in the solution of the Hamiltonian given by Eq. (1). Making the substitution  $k_z \rightarrow -i \frac{d}{dz}$ , we start by writing the  $8 \times 8$  Hamiltonian for the superlattice as a set of eight coupled equations:

$$\sum_{n'=1}^8 H_{nn'} \left( z, k_x, k_y, -i \frac{d}{dz} \right) F_{n'}(z) = E F_n(z). \quad (\text{A1})$$

The one-dimensional envelope functions  $F_n(z)$  are expanded into a discrete Fourier series:

$$F_n(z) = \sum_{j=-j_{\max}}^{j_{\max}} F_n(j) \phi_j(z), \quad (\text{A2})$$

where

$$\phi_j(z) = \frac{1}{\sqrt{L}} e^{i \frac{2\pi}{L} (j+q_z) z}, \quad (\text{A3a})$$

$$j_{\max} = \frac{L}{a_{\text{av}}}. \quad (\text{A3b})$$

$L$  is the superlattice period and  $a_{\text{av}}$  is the average cubic lattice constant in the growth direction. The summation in Eq. (A2) has been limited to  $j_{\max}$  so that only Fourier components within the first bulk Brillouin zone are included. This reflects the Fourier makeup of the envelope functions which are exact solutions of the  $k$ -space Hamiltonian.<sup>17,20</sup> It should be noted, however, that in the transformation to real space, the limitation of Fourier components to the first Brillouin zone was dropped. This resulted in a real-space Hamiltonian whose exact mathematical solution requires envelope functions with all Fourier components. Takhtamirov and Volkov argued that the contributions with  $j > j_{\max}$  should correspond to corrections

of order  $\ell \geq 2$ ,<sup>20</sup> in which case they are small enough to be neglected. In Sec. VI, solutions with  $j \leq j_{\max}$  and  $j' \leq j'_{\max}$  are discussed, where  $j'_{\max} \rightarrow \infty$ , and it is shown that the difference between the two solutions, both of which are approximations to the exact solution, is in fact quite significant.

The parameter  $q_z$  is inserted in order to satisfy Bloch's theorem that in the  $z$  direction,

$$F_n(z+L) = F_n(z) e^{iq_z L}, \quad (\text{A4})$$

where  $q_z$  is defined as  $q = \frac{2\pi q_z}{L}$  and spans the entire mini-Brillouin zone of the superlattice ( $-0.5 \leq q_z \leq 0.5$ ).

The set of coupled differential equations in Eq. (A1) can be converted into a set of coupled algebraic equations by multiplying by  $\phi_j^*(z)$  and integrating over the superlattice period. The result is

$$\sum_{n'=1}^8 \sum_{j'=-j_{\max}}^{j_{\max}} H_{nn'}(j+q_z, j'+q_z) F_{n'}(j'+q_z) = E F_n(j+q_z), \quad (\text{A5})$$

where

$$H_{nn'}(j+q_z, j'+q_z) = \int dz \phi_{j+q_z}^*(z) H_{nn'}(z, k_x, k_y, k_z) \phi_{j'+q_z}(z). \quad (\text{A6})$$

When performing the Fourier-transform integral for  $H_{nn'}$ , we need to remember that the superlattice is constructed of two materials (A and B) and two interfaces (B on A, labeled BA, and A on B, labeled AB). We can divide the integral into four parts:

$$\int_{\text{period}} = \int_{\epsilon}^{L_A-\epsilon} + \int_{L_A-\epsilon}^{L_A+\epsilon} + \int_{L_A+\epsilon}^{L_A+L_B-\epsilon} + \int_{L_A+L_B-\epsilon}^{L_A+L_B+\epsilon}, \quad (\text{A7})$$

where  $\epsilon \rightarrow 0$  indicates the interface layer. The first and third integrals are on materials A and B, respectively, and the second and fourth integrals are on the BA and AB interfaces, respectively. All yield simple linear or exponential terms which depend on the Fourier indices  $j$  and  $j'$  and the coordinates of the interfaces.

The dispersion relation is obtained by diagonalizing the Hamiltonian [Eq. (A5)], with different values of  $k_x$ ,  $k_y$ , and  $q_z$ .

### 2. Transition oscillator strength

The oscillator strength for a given energy transition can be calculated by taking the square of the absolute value of the optical matrix element of the selected transition. The optical matrix element is given by

$$M_{v,c} = \langle \Psi_c(z) | \hat{e} \cdot \frac{\hbar}{i} \nabla | \Psi_v(z) \rangle, \quad (\text{A8})$$

where  $\hat{e}$  is the polarization vector of the optical electric field and  $\Psi_v$  and  $\Psi_c$  are the wave functions of the hole and electron states, respectively, involved in the transition. At this stage, we assume that these wave functions have the general form  $\sum_{n=1}^8 F_n(z) u_n(\mathbf{r})$ , where  $u_n(\mathbf{r})$  is a zone-center Bloch state of the bulk reference crystal.

When we insert the wave functions into Eq. (A8), we obtain

$$M_{v,c} = \sum_{n,n'=1}^8 \sum_j \sum_{j'} F_{n,j}^{c*} F_{n',j}^v \times \int \phi_j^*(z) u_n^*(\mathbf{r}) \hat{e} \cdot \frac{\hbar}{i} \nabla [\phi_{j'}(z) u_{n'}(\mathbf{r})] d^3 r. \quad (\text{A9})$$

The integral can be written as

$$\int \phi_j^*(z) \phi_{j'}(z) \cdot u_n^*(\mathbf{r}) \hat{e} \cdot \frac{\hbar}{i} \nabla u_{n'}(\mathbf{r}) d^3 r + \int u_n^*(\mathbf{r}) u_{n'}(\mathbf{r}) \cdot \phi_j^*(z) \hat{e} \cdot \frac{\hbar}{i} \nabla \phi_{j'}(z) d^3 r. \quad (\text{A10})$$

Let us denote the first integral  $I_1$ . Under the assumption discussed above, that the Fourier components of the envelope functions lying outside the first bulk Brillouin zone are small enough to be ignored, the integral can be separated into the product of integrals over the superlattice unit cell and the bulk unit cell of the reference crystal:<sup>4</sup>

$$I_1 = \frac{\hbar}{i} \int_{\text{SL cell}} \phi_j^*(z) \phi_{j'}(z) dz \int_{\text{Bulk cell}} u_n^*(\mathbf{r}) \times \sum_{i=x,y,z} e_i \frac{\partial}{\partial i} u_{n'}(\mathbf{r}) d^3 r. \quad (\text{A11})$$

Substituting the expression for  $\phi$  in Eq. (A3a), and noting that the  $P$  parameter of the reference crystal is  $P = -i \frac{\hbar}{m_0} \langle u_S | p_x | u_X \rangle$ , this expression becomes

$$I_1 = iP \frac{m_0}{\hbar} \delta_{jj'} \times \sum_{i=X,Y,Z} \left[ e_i \sum_{k=\uparrow,\downarrow} (\delta_{n,S_k} \delta_{n',i_k} - \delta_{n,i_k} \delta_{n',S_k}) \right], \quad (\text{A12})$$

where we only consider near-band-gap optical transitions between  $p$ -like valence states and  $s$ -like conduction states. The two summations are over three polarization directions and two electron spin directions. For example, the first element in the double summation is  $i = X$  and  $k = \uparrow$ . In this case, the sum argument is

$$\delta_{n,S\uparrow} \delta_{n',X\uparrow} - \delta_{n,X\uparrow} \delta_{n',S\uparrow}.$$

The second integral in Eq. (A10), denoted  $I_2$ , is zero for optical polarization in the plane when considering interband transitions.

Finally, the oscillator strength  $S_{v,c}$  is given by

$$S_{v,c} = |M_{v,c}|^2 = \left( \eta P \frac{m_0}{\hbar} \right)^2 \times \left| \sum_{j=-j_{\max}}^{j_{\max}} \sum_{i=X,Y,Z} \left[ e_i \sum_{k=\uparrow,\downarrow} (F_{S_k,j}^{c*} F_{i_k,j}^v - F_{i_k,j}^{c*} F_{S_k,j}^v) \right] \right|^2. \quad (\text{A13})$$

$\eta$  is an empirical constant, inserted to account for the fact that the basis wave functions of the  $8 \times 8$  Hamiltonian are not in fact pure  $S$ ,  $X$ ,  $Y$ , and  $Z$  orbitals of the reference crystal, but contain small (spatially dependent) admixtures of other

TABLE II. Material parameters of InAs and GaSb used in the calculations for temperatures of 77 and 300 K. All values, except  $E_p$ , were taken from Refs. 27 and 28. The  $E_p$  values are close to those predicted by Lawaetz (Ref. 29) and were determined independently (Ref. 37) by the five-band  $\mathbf{k} \cdot \mathbf{p}$  treatment discussed in Appendix C. The temperature dependence of the lattice parameters has negligible influence on our results and has been ignored.

Parameter	77 K		300 K	
	InAs	GaSb	InAs	GaSb
$a_0$ (Å)	6.0584	6.0954	6.0584	6.0954
$E_0$ (eV)	0.418	0.814	0.359	0.725
$\Delta_0$ (eV)	0.38	0.76	0.38	0.76
$E'_0$ (eV)	4.52	3.2	4.52	3.2
$\Delta'_0$ (eV)	0.175	0.4	0.175	0.4
$E_p$ (eV)	22.42	22.75	22.19	23.47
$m_e^*$	0.022	0.042	0.019	0.037
$c_{11}$ (GPa)	832.9	884.2	832.9	884.2
$c_{12}$ (GPa)	452.6	402.6	452.6	402.6
$a_c$ (eV)	-5.08	-6.85	-5.08	-6.85
$a_v$ (eV)	1.0	0.79	1.0	0.79
$b$ (eV)	-1.8	-2.0	-1.8	-2.0

zone-center states, as a result of the transformation that is used to reduce the infinite  $\mathbf{k} \cdot \mathbf{p}$  Hamiltonian to a Hamiltonian of eight bands.<sup>11,17</sup> To treat these basis functions properly would introduce many additional unknown interaction parameters with remote bands, and is not practically useful.

## APPENDIX B: CALCULATION PARAMETERS

The bulk material parameters that were used in the calculations, and the sources from which they were obtained, are given in Table II.

The  $\mathbf{k} \cdot \mathbf{p}$  parameters that were deduced by fitting the TVK8 model to experimental data are given in Table III. The fitting procedure is described in Sec. V. Note that the only Luttinger parameters that are independent at a given temperature are  $\gamma_1$  and  $\gamma_2$  for InAs. All others are marked with a superscript ‘‘a’’ to indicate that they have been calculated from the independent

TABLE III. Fitted  $\mathbf{k} \cdot \mathbf{p}$  parameters of InAs and GaSb used in the calculations, for temperatures of 77 and 300 K. Valence band offsets of the unstrained materials (VBO) are relative to the GaSb VB.

Parameter	77 K		300 K	
	InAs	GaSb	InAs	GaSb
$\alpha$ (eVÅ)	0.2		0.2	
$\beta$ (eVÅ)	0.2		0.2	
$D_S$ (eVÅ)	3		2.9	
$D_X$ (eVÅ)	1.3		1.5	
$D_Z$ (eVÅ)	1.1		1.3	
$\gamma_1$	20.0	11.87 <sup>a</sup>	23.8	14.48 <sup>a</sup>
$\gamma_2$	9.0	4.61 <sup>a</sup>	10.7	5.67 <sup>a</sup>
$\gamma_3$	9.16 <sup>a</sup>	4.99 <sup>a</sup>	10.39 <sup>a</sup>	5.60 <sup>a</sup>
VBO (eV)	-0.560	0	-0.501	0

<sup>a</sup>Not independent parameters: calculated from  $\gamma_1$  and  $\gamma_2$  of InAs using the method described in Appendix C.

ones according to the method described in Appendix C. The interface parameters must be used with  $\pi_i = +1$  for the GaSb on InAs interface ( $\pi_i = -1$  for InAs on GaSb).

### APPENDIX C: CONSTRAINTS ON THE LUTTINGER PARAMETERS FOR NEARLY LATTICE MATCHED SUPERLATTICES

In Eq. (33) of Ref. 17, one of the authors proposed a set of constraint relations to predict four out of the six Luttinger parameters in an unstrained superlattice from the other two, with an accuracy of  $\ell = 2$ . We now consider how to apply the constraint relations when one of the superlattice materials is slightly strained, for example, in an InAs/GaSb type-II superlattice grown on GaSb. As discussed in Sec. V, this allows us to reduce the number of independent fitting parameters in our model.

In Ref. 17, it was suggested that before applying the constraint relations, the InAs should first be deformed hydrostatically, in order to achieve a perfect lattice match with GaSb, and that  $E_P$  and all the band gaps should be adjusted, according to the known deformation potentials and strain values. We shall term the hydrostatically deformed material InAs'. Based on the following argument, we show that an even simpler approach can be used, where the constraint relations are applied directly to the unstrained pair of materials.

The constraint relations were derived for a superlattice A/B/A/B/..., which is assumed to be perfectly lattice matched.<sup>17</sup> They are based on four equations involving the Kane parameters  $F'$ ,  $H_1$ , and  $G$  associated with the  $s$ ,  $p$ , and  $d$  bands, respectively:<sup>46</sup>  $F'_A \approx 0$ ,  $F'_B \approx 0$ ,  $H_{1B} - H_{1A} \approx \chi H_{1A}$  and  $G_B - G_A \approx 0$ , where  $\chi = 1 - \frac{E'_G(B)}{E'_G(A)}$  and  $E'_G$  is the band gap between bonding and antibonding  $p$  states in the absence of the spin-orbit interaction ( $E'_G = E_{\Gamma_{15c}} - E_{\Gamma_{15v}}$ ). For a small amount of strain, such as the  $\sim 0.6\%$  between InAs and InAs', the changes in  $H_1$  and  $G$  turn out to be negligible (typically

$<2\%$ ), due to the relatively large band gaps that appear in the denominators of these parameters. In addition,  $F' \approx 0$  for any cubic narrow band-gap material, so this applies equally well to InAs or InAs'. Thus, since none of the three Kane parameters change significantly between InAs and InAs', the constraint relations can be applied directly to unstrained InAs, i.e., the above four equations still hold with sufficient accuracy, when A and B represent the unstrained materials.

In order to be consistent with standard definitions for the Luttinger parameters of narrow band-gap materials,<sup>29,47,48</sup> Klipstein's  $\gamma_4$  parameter should be written as  $\gamma_4 = \frac{E_P}{E_0}$ , where  $E_0$  is the fundamental band gap.<sup>49</sup> As will be discussed below,  $\gamma_4$  can be determined quite accurately in both materials, using spectroscopic data in a bulk five-band  $\mathbf{k} \cdot \mathbf{p}$  model. Thus, the Luttinger parameters  $\gamma_1^A$  and  $\gamma_2^A$  (for material A) turn out to be the only independent Luttinger parameters, because Eq. (33) of Ref. 17 can be rearranged to express the other Luttinger parameters in terms of the four parameters:  $\gamma_1^A$ ,  $\gamma_2^A$ ,  $\gamma_4^A$  and  $\gamma_4^B$  as follows:

$$\gamma_3^A \approx \frac{1}{12} + \frac{1}{12}\gamma_1^A - \frac{2}{3}\gamma_2^A + \frac{\gamma_4^A}{4}, \quad (\text{C1a})$$

$$\gamma_1^B \approx \frac{2\chi}{3} + \left(1 + \frac{2\chi}{3}\right)\gamma_1^A - \frac{4}{3}\chi\gamma_2^A - \frac{1}{3}\gamma_4^A + \frac{1}{3}\gamma_4^B, \quad (\text{C1b})$$

$$\gamma_2^B = -\frac{\chi}{6} - \frac{\chi}{6}\gamma_1^A + \left(1 + \frac{\chi}{3}\right)\gamma_2^A - \frac{1}{6}\gamma_4^A + \frac{1}{6}\gamma_4^B, \quad (\text{C1c})$$

$$\gamma_3^B = \left(\frac{2\chi + 1}{12}\right) + \left(\frac{2\chi + 1}{12}\right)\gamma_1^A - \left(\frac{\chi + 2}{3}\right)\gamma_2^A + \frac{1}{12}\gamma_4^A + \frac{1}{6}\gamma_4^B. \quad (\text{C1d})$$

Table IV shows the Luttinger parameters deduced from the preceding equations for several pairs of nearly lattice matched materials, and compares them with the widely used values

TABLE IV. Using Eqs. (C1a)–(C1d) for pairs of nearly lattice matched semiconductors at 77 K, the four Luttinger parameters with a superscript ‘‘a’’ are calculated from the two independent Luttinger parameters. The latter are adjusted until the error relative to the Lawaetz (Ref. 29) values is minimized, as shown in the last three rows. The band-gap parameters for the calculation are listed in the first five rows. For the binary materials, these are based on Refs. 27 and 28 and are close or equal to those used by Lawaetz (Ref. 29). For  $\text{In}_{0.57}\text{Ga}_{0.47}\text{As}$ , bowing parameters were used for  $E_0$ ,  $\Delta_0$ , and  $E_P$ , taken from Ref. 36. The Luttinger parameters shown in parentheses for  $\text{In}_{0.57}\text{Ga}_{0.47}\text{As}$  were calculated using the interpolation method proposed by Vurgaftman *et al.* (Ref. 36).

	GaAs	AlAs	GaSb	AlSb	InAs	GaSb	$\text{In}_{0.53}\text{Ga}_{0.47}\text{As}$	InP
$E_0$ (eV)	1.519	3.13	0.814	2.32	0.418	0.814	0.817	1.424
$\Delta_0$ (eV)	0.34	0.28	0.76	0.65	0.38	0.76	0.32	0.108
$E'_0$ (eV)	4.488	4.34	3.2	3.7	4.52	3.2	4.52	4.8
$\Delta'_0$ (eV)	0.171	0.14	0.4	0.3	0.18	0.4	0.19	0.065
$E_P$ (eV)	25.7	21.1	22.4	18.7	22.2	22.4	24.2	20.4
$\gamma_1$	7.4	4.1 <sup>a</sup>	11.14	4.38 <sup>a</sup>	19.8	11.84 <sup>a</sup>	11.45 (10.9)	6.29 <sup>a</sup>
$\gamma_2$	2.48	0.76 <sup>a</sup>	4.16	0.98 <sup>a</sup>	8.45	4.04 <sup>a</sup>	4.65 (4.1)	2.11 <sup>a</sup>
$\gamma_3$	3.28 <sup>a</sup>	1.6 <sup>a</sup>	5.12 <sup>a</sup>	1.81 <sup>a</sup>	9.38 <sup>a</sup>	5.25 <sup>a</sup>	5.35 <sup>a</sup> (5.0)	2.78 <sup>a</sup>
$\Delta\gamma_1$ (%)	−3.3	+1.5	−5.6	+5.6	+0.7	+0.3		+0.1
$\Delta\gamma_2$ (%)	+2.9	−2.5	+3.2	−2.5	+1.0	+0.3		+1.4
$\Delta\gamma_3$ (%)	−0.1	2.1	−2.7	3.3	+0.9	−0.1		+0.8

<sup>a</sup>Not independent parameters: calculated from  $\gamma_1$  and  $\gamma_2$  of the narrower band-gap material.

of Lawaetz.<sup>29</sup> With the exception of InGaAs/InP, which is discussed below, the Luttinger parameters  $\gamma_1$  and  $\gamma_2$  of the material with the narrower band gap were chosen to be close to the Lawaetz values<sup>29</sup> and were used to calculate the  $\gamma_3$  value of the narrower band-gap material (left-hand column) and the  $\gamma_1$ ,  $\gamma_2$ , and  $\gamma_3$  values of the wider band-gap material (right-hand column). These four calculated values also turn out to agree quite well with the corresponding values determined by Lawaetz. The quality of the agreement is discussed further in the following.

Table IV also lists the band-gap values for  $E_0$  ( $\Gamma_{6c} - \Gamma_{8v}$ ),  $\Delta_0$  ( $\Gamma_{8v} - \Gamma_{7v}$ ),  $E'_0$  ( $\Gamma_{7c} - \Gamma_{8v}$ ), and  $\Delta'_0$  ( $\Gamma_{8c} - \Gamma_{7c}$ ) that were used in the calculation. They are close to the experimentally determined values quoted both by Lawaetz<sup>29</sup> and also in more recent data sources.<sup>27,28</sup> Note that  $E'_G = E'_0 + \frac{2\Delta'_0}{3} + \frac{\Delta_0}{3}$ . The values of  $E_P$  listed in Table IV for the six binary materials are those due to Lawaetz.<sup>29</sup> For the direct band-gap materials, they are within a few percent of the values that we have determined experimentally using a five-level  $\mathbf{k} \cdot \mathbf{p}$  treatment<sup>50,51</sup> and spectroscopic data.<sup>37</sup> Although we use the latter in our model (see Table II), we consider the Lawaetz values to be very close to ours and so use his values here without modification, in order to be more consistent in our comparison with his Luttinger parameters.

For  $\text{In}_{0.57}\text{Ga}_{0.47}\text{As}$ , weighted averages of the band gap and  $E_P$  values of InAs and GaAs were calculated, after which  $E_0$ ,  $\Delta_0$ , and  $E_P$  were modified according to the bowing parameters given by Vurgaftman *et al.*<sup>36</sup> for the alloy.  $\gamma_1$ ,  $\gamma_2$ , and  $\gamma_3$  of  $\text{In}_{0.57}\text{Ga}_{0.47}\text{As}$  were then calculated in two ways: first, by varying  $\gamma_1$  and  $\gamma_2$  until the three Luttinger parameters of InP obtained using Eqs. (C1a)–(C1d) were all within 1% of those quoted by Lawaetz;<sup>29</sup> second, by using the method proposed by Vurgaftman *et al.*, where  $\gamma_1$ ,  $\gamma_2$ , and  $\gamma_3$  are deduced from linear interpolations of the quantity  $\gamma_2 - \gamma_3$ , and the heavy- and light-hole effective masses along [001]. The Luttinger parameters determined in this way are shown in parentheses.

The last three lines in Table IV give the error in the Luttinger parameters of the binary materials relative to those determined by Lawaetz.<sup>29</sup> It may be seen that it is possible to find values for two independent Luttinger parameters such that the error in these and the four computed Luttinger parameters is less than 6% in all cases, and usually, it is considerably smaller.<sup>52</sup> Table IV thus provides good support for the approach adopted in this work, where only  $\gamma_1$  and  $\gamma_2$  of InAs are used as independent fitting parameters, when making comparisons with experimental data. It shows that the four computed Luttinger parameters should be close to their expected values. Nevertheless, we do not simply use the six Lawaetz values in our model, unchanged, since this gives a poorer fit to our measured absorption spectra and photoluminescence data than using our fitting procedure based on two parameters. This is true even though our fitted values for InAs of  $\gamma_1 = 20.0$  and  $\gamma_2 = 9.0$  in Table III differ from the Lawaetz values by less than 8%. We do not expect precise agreement due to the different approximations used in each work. However, it does highlight the sensitivity of the calculated absorption spectrum to even small changes in these parameters and hence the importance of using the correct fitting procedure.

Finally, the good consistency between the calculated values of the InP Luttinger parameters in Table IV and the Lawaetz values gives some confidence that our approach of determining the Luttinger parameters for the ternary alloy, based on Eqs. (C1a)–(C1d), may be a better method than that proposed by Vurgaftman *et al.*,<sup>36</sup> whose values, shown in parentheses, are lower by up to 12%. Presumably, this is because the linear interpolation of the masses in the Vurgaftman *et al.* treatment does not properly take bowing effects into account. We note that the difference between the two approaches is even more significant for superlattice systems such as InAs/InAs<sub>1-x</sub>Sb<sub>x</sub> lattice matched to GaSb, where the constituent materials have smaller band gaps and the band-gap bowing in the alloy is much stronger.<sup>53–55</sup>

\*yoavlivn@post.tau.ac.il

†philip\_k@scd.co.il

<sup>1</sup>D. M. Wood and A. Zunger, *Phys. Rev. B* **53**, 7949 (1996).

<sup>2</sup>L. C. Lew Yan Voon and M. Willatzen, *The k·p Method: Electronic Properties of Semiconductors* (Springer, Berlin, 2009).

<sup>3</sup>E. O. Kane, *J. Phys. Chem. Solids* **1**, 82 (1956); *Semicond. Semimet.* **1**, 75 (1966).

<sup>4</sup>J. M. Luttinger and W. Kohn, *Phys. Rev.* **97**, 869 (1955).

<sup>5</sup>D. L. Smith and C. Mailhot, *Phys. Rev. B* **33**, 8345 (1986).

<sup>6</sup>M. G. Burt, *J. Phys.: Condens. Matter* **4**, 6651 (1992).

<sup>7</sup>See, for example, Fig. 8 of Ref. 6.

<sup>8</sup>B. A. Foreman, *Phys. Rev. Lett.* **81**, 425 (1998).

<sup>9</sup>I. Aleiner and E. Ivchenko, *Pis'ma Zh. Eksp. Teor. Fiz.* **55**, 662 (1992) [*JETP Lett.* **55**, 692 (1992)].

<sup>10</sup>B. A. Foreman, *Phys. Rev. B* **48**, 4964 (1993).

<sup>11</sup>É. E. Takhtamirov and V. A. Volkov, *Semicond. Sci. Technol.* **12**, 77 (1997).

<sup>12</sup> $ka$  should typically be about  $1-2 \times \pi/N_{ml}$  where  $N_{ml}$  is the number of monolayers in a superlattice period.

<sup>13</sup>O. Krebs and P. Voisin, *Phys. Rev. Lett.* **77**, 1829 (1996).

<sup>14</sup>O. Krebs, D. Rondi, J. L. Gentner, L. Goldstein, and P. Voisin, *Phys. Rev. Lett.* **80**, 5770 (1998).

<sup>15</sup>H. Im, P. C. Klipstein, R. Grey, and G. Hill, *Phys. Rev. Lett.* **83**, 3693 (1999).

<sup>16</sup>T. Reker, H. Im, L. E. Bremme, H. Choi, Y. Chung, P. C. Klipstein, and H. Shtrikman, *Phys. Rev. Lett.* **88**, 056403 (2002).

<sup>17</sup>P. C. Klipstein, *Phys. Rev. B* **81**, 235314 (2010).

<sup>18</sup>L. Leibler, *Phys. Rev. B* **12**, 4443 (1975).

<sup>19</sup>V. A. Volkov and É. E. Takhtamirov, *Usp. Fiz. Nauk.* **167**, 1123 (1997) [*Phys. Usp.* **40**, 1071 (1997)].

<sup>20</sup>É. E. Takhtamirov and V. A. Volkov, *Zh. Eksp. Teor. Fiz.* **116**, 1843 (1999) [*JETP* **89**, 1000 (1999)].

<sup>21</sup>G. A. Sai-Halasz, R. Tsu, and L. Esaki, *Appl. Phys. Lett.* **30**, 651 (1977).

<sup>22</sup>J. Rodriguez, C. Cervera, and P. Christol, *Appl. Phys. Lett.* **97**, 251113 (2010).

<sup>23</sup>P. Manurkar, S. Ramezani-Darvish, B.-M. Nguyen, M. Razeghi, and J. Hubbs, *Appl. Phys. Lett.* **97**, 193505 (2010).

- <sup>24</sup>R. Rehm, M. Walther, F. Rutz, J. Schmitz, A. Worl, J.-M. Masur, R. Scheibner, J. Wendler, and J. Ziegler, *J. Electron. Mater.* **40**, 1738 (2011).
- <sup>25</sup>A. Ongstad, R. Kaspi, C. Moeller, M. Tilton, D. Gianardi, J. Chavez, and G. Dente, *J. Appl. Phys.* **89**, 2185 (2001).
- <sup>26</sup>G. C. Dente and M. L. Tilton, *Phys. Rev. B* **66**, 165307 (2002).
- <sup>27</sup>*Physics of Group IV Elements and III-V Compounds*, Landolt-Börnstein New Series, Group III, Vol. 17, edited by K. H. Hellwege and O. Madelung (Springer, Berlin, 1982).
- <sup>28</sup>*Intrinsic Properties of Group IV Elements and III-V, II-VI and I-VII Compounds*, Landolt-Börnstein New Series, Group III, Vol. 22, edited by O. Madelung (Springer, Berlin, 1987).
- <sup>29</sup>P. Lawaetz, *Phys. Rev. B* **4**, 3460 (1971).
- <sup>30</sup>D. Gershoni, C. Henry, and G. A. Baraff, *IEEE J. Quantum Electron.* **29**, 2433 (1993).
- <sup>31</sup>G. Pikus and G. Bir, *Symmetry and Strain Induced Effects in Semiconductors* (Wiley, New York, 1974).
- <sup>32</sup>B. Sapati, J. Rodrigues, A. Trampert, E. Tournie, A. Joullie, and P. Christol, *J. Cryst. Growth* **301-302**, 889 (2007).
- <sup>33</sup>The wedges are truncated except those with a vertex at the zone center.
- <sup>34</sup>The reason we can use only half of the  $k_x$ - $k_y$  plane is because of the  $180^\circ$  rotational symmetry of the zinc-blende structure.
- <sup>35</sup>F. Szmulowicz, H. Haugan, and G. J. Brown, *Phys. Rev. B* **69**, 155321 (2004).
- <sup>36</sup>I. Vurgaftman, J. R. Meyer, and L. R. Ram-Mohan, *J. Appl. Phys.* **89**, 5815 (2001).
- <sup>37</sup>P. Klipstein, Y. Livneh, O. Klin, S. Grossman, N. Snapi, A. Glozman, and E. Weiss, *Infrared Phys. Technol.* (to be published).
- <sup>38</sup>W. Lau and M. Flatte, *Appl. Phys. Lett.* **80**, 1683 (2002).
- <sup>39</sup>B. A. Foreman, *Phys. Rev. B* **72**, 165345 (2005).
- <sup>40</sup>I. Semenikhin, A. Zakharova, and K. A. Chao, *Phys. Rev. B* **77**, 113307 (2008).
- <sup>41</sup>These authors did not specify the interface type.
- <sup>42</sup>I. Semenikhin, A. Zakharova, and K. Chao, *Semicond. Sci. Technol.* **23**, 125044 (2008).
- <sup>43</sup>L. L. Li, W. Xu, and F. M. Peeters, *Phys. Rev. B* **82**, 235422 (2010).
- <sup>44</sup>B. H. Hong, S. I. Rybchenko, I. E. Itskevich, S. K. Haywood, R. Intartaglia, V. Tasco, G. Rainò, and M. De Giorgi, *Phys. Rev. B* **79**, 165323 (2009).
- <sup>45</sup>The fitted band overlap is expressed to three significant figures because this level of accuracy is needed to obtain the best fit to the measured layer widths and band gaps. However, the typical error between the fitted and the true band overlap values can only be quoted to two significant figures.
- <sup>46</sup>Klipstein uses the notation  $F'$  ( $6 \times 6$ ) and  $F''$  ( $8 \times 8$ ) for Kane's  $F$  and  $F'$  parameters, respectively.
- <sup>47</sup>M. Weiler, *J. Magn. Magn. Mater.* **11**, 131 (1979).
- <sup>48</sup>C. Pidgeon and R. Brown, *Phys. Rev.* **146**, 575 (1966).
- <sup>49</sup>This also removes the apparent discrepancy in Klipstein (Ref. 17) where the value of the Kane  $F$  parameter in both InAs and GaSb appeared to be too large.
- <sup>50</sup>M. Cardona, N. E. Christensen, and G. Fasol, *Phys. Rev. B* **38**, 1806 (1988).
- <sup>51</sup>Note that the first sign on the second line of Eq. (2.4) in Ref. 50 should be changed to a minus. The correct equation can be found, for example, as Eq. (3.7) in Ref. 56.
- <sup>52</sup>This reasonable agreement between our treatment, based on two independent parameters, and Lawaetz's treatment of all six parameters, can be related to the fact that in both approaches it is the band-gap changes that have the most dominant effect on the Kane parameters, while the effect of the momentum matrix elements is much smaller (Ref. 17).
- <sup>53</sup>S. Cripps, T. Hosea, A. Krier, V. Smirnov, P. Batty, Q. Zhuang, H. Lin, P.-W. Liu, and G. Tsai, *Thin Solid Films* **516**, 8049 (2008).
- <sup>54</sup>E. Steenbergen, B. C. Connelly, G. D. Metcalfe, H. Shen, M. Wraback, D. Lubyshev, Y. Qui, J. M. Fastenau, A. Liu, S. Elhamri, O. Cellek, and Y.-H. Zhang, *Appl. Phys. Lett.* **99**, 251110 (2011).
- <sup>55</sup>W. L. Sarney, S. P. Svensson, H. Hier, G. Kipshidze, D. Donetsky, D. Wang, L. Shterengas, and G. Belenky, *J. Vac. Sci. Technol.* **30**, 02B105 (2012).
- <sup>56</sup>T. E. Ostromek, *Phys. Rev. B* **54**, 14467 (1996).